

Cavity perturbation by superconducting films in microwave magnetic and electric fields

D.-N. Peligrad,^{*,†} B. Nebendahl, C. Kessler,[‡] and M. Mehring
Physikalisches Institut, Universität Stuttgart, D-70550 Stuttgart, Germany

A. Dulčić[§] and M. Požek

*Department of Physics, Faculty of Science and Ruđer Bošković Institute, P.O. Box 162, HR-10001 Zagreb, Croatia
 and Physikalisches Institut, Universität Stuttgart, D-70550 Stuttgart, Germany*

D. Paar

Department of Physics, Faculty of Science and Ruđer Bošković Institute, P.O. Box 162, HR-10001 Zagreb, Croatia

(Received 23 March 1998)

Cavity perturbation by superconducting films is treated in a unified way for the sample positions in both magnetic and electric microwave fields. The role of demagnetizing and depolarizing effects in the boundary conditions of the fields is analyzed. The general solutions for the complex frequency shift are specified for the samples having slab geometry and the field being parallel to the plane of the sample. For electromagnetically thick samples, the shifts for samples placed in the magnetic and electric fields are found to have the same magnitude and temperature dependence, while for thin films dramatic differences are obtained. The magnitude of the shift is reduced in the magnetic and increased by orders of magnitude in the electric field. A remarkable feature in the temperature dependence of the real frequency shift in the electric field is obtained. Experiments are performed on an $\text{YBa}_2\text{Cu}_3\text{O}_{7-\delta}$ thin film, and all the predictions of the theory are confirmed. It is also shown that microwave cavity perturbation and ac susceptibility measurements in a dc magnetic field can be covered by the same theory. Their profoundly different temperature dependence can be accounted for by their different frequencies. [S0163-1829(98)05741-5]

I. INTRODUCTION

Microwave and millimeter-wave measurements on thin films of high- T_c superconductors were carried out by a number of research groups¹⁻¹⁸ using different experimental techniques involving resonant structures. From the technological point of view it is important to determine the losses of a fabricated thin film and compare it with those of copper. The potential applications would include resonators, filters, delay lines, couplers, and antenna matching networks with benefits of improved performance, reduced size, and weight in, e.g., satellite communication receivers. On the more fundamental scientific side it is interesting to reveal the temperature-dependence of the complex conductivity, which governs the response of the superconductor to the microwave field. For a superconductor in the Meissner state the temperature dependent complex conductivity $\tilde{\sigma} = \sigma_1 - i\sigma_2$ is due to the quasi-particles and condensed superconducting pairs. In the mixed state one also has to take into account the contribution of vortex oscillations resulting in an effective complex conductivity,^{19,20} which is both temperature and field dependent. The latter can be used to determine the upper critical field²¹ or to study pinning effects.²² In what follows we shall for simplicity restrict ourselves first to the notation of the Meissner state giving examples of temperature-dependent $\tilde{\sigma}$. In later sections we point out that the theory is valid also for the more complicated effective conductivity of the mixed state.

There is an important difference between measurements of thick samples (usually single crystals) and thin samples

(typically thin films). For a sample which is much thicker than the microwave penetration depth, a simple relation holds between the complex conductivity and the complex surface impedance

$$\tilde{Z}_s = \sqrt{i \frac{\mu_0 \omega}{\sigma_1 - i\sigma_2}} = R_s + iX_s, \quad (1)$$

which is called intrinsic because it depends only on the material property and not on the sample dimensions. Experiments based on resonant cavities or other resonant structures usually yield changes of the Q factor and frequency shift, which can be related to the values of the real (R_s) and imaginary (X_s) part of Z_s wherefrom σ_1 and σ_2 are readily deduced.

However, for samples whose thickness is comparable or even smaller than the microwave penetration depth, the measured Q factor and frequency shift do not yield directly the intrinsic values of R_s and X_s . Formally, one can still denote the measured quantities as R and X , but these depend in a nontrivial way on the intrinsic R_s and X_s and the sample thickness. The usual thickness of high- T_c thin films ranges from 100–500 nm. Given the resistivity of these superconductors above T_c (about $0.5 \mu\Omega \text{ m}$), the microwave (10–100 GHz) penetration depth exceeds the film thickness in the normal state and just below T_c . Hence, the sample is electromagnetically thin in this range of temperatures. Upon cooling the penetration depth may be reduced below the sample thickness and the sample becomes electromagnetically thick at very low temperatures. This transition entails complications in the determination of σ_1 and σ_2 .

Several experimental arrangements for the microwave measurements of thin films have been described in the literature. One of them consists in replacing the end wall of the microwave cavity by a thin film sample.¹⁻⁷ Near T_c and above where the penetration depth is larger than the film thickness, there is a considerable leakage of the microwave power from the cavity through the thin film. Impedance transformation theory was used to find the effective impedance \tilde{Z}_{eff} on the inner side of the thin film. It includes the intrinsic impedances and phase shifts in the superconducting thin film, in the dielectric substrate, and in the vacuum behind it.^{4,5} In order to extract the intrinsic R_s and X_s of the superconducting thin film from the measured R_{eff} and X_{eff} , it is necessary to have a very precise knowledge of the electric permittivity of the substrate including its temperature dependence. Even then one obtains a complicated set of equations for arbitrary σ_1 and σ_2 , which can be simplified in the limit of $\sigma_2 \gg \sigma_1$, i.e., only at low temperatures.⁵ A complete evaluation of the temperature dependence of $\tilde{\sigma}$ including the behavior at the superconducting transition becomes quite uncertain for thin films in this experimental arrangement.

Radiation losses can be minimized in stripline resonators with two ground planes.⁹ Still, for the penetration depth comparable or larger than the film thickness, some geometrical factors must be evaluated, and the determination of $\tilde{\sigma}$ at higher temperatures is less accurate. The use of a parallel plate resonator is also convenient only at low temperatures.¹⁷

Intracavity arrangements where the sample is placed inside a resonant cavity are particularly attractive because no energy is radiated through the sample out of the cavity. Two choices can be made for the intracavity position of the sample. The first is that the sample is at the position of the magnetic field maximum¹⁰⁻¹² while the other choice is the electric field maximum.^{13,14} The problem is reduced to the cavity perturbation by the superconducting thin film.

In the present paper we analyze the perturbation conditions for the two intracavity positions and point out the differences which were not considered before. We start from the conventional perturbation theory for paramagnetic and dielectric samples and show how it can be modified to allow the treatment of metallic samples. For the sake of completeness we present the resulting perturbation expressions with the induced current in the sample treated as both a bound current and a free one. Analytical solutions are found for the slab geometry of the sample with profoundly different behavior in magnetic and electric fields. In order to provide experimental support to the theory we present results on a thin superconducting film of $\text{YBa}_2\text{Cu}_3\text{O}_{7-\delta}$ placed successively at various positions from the magnetic to the electric field maximum. All the features predicted by the theory have been confirmed.

We also show that microwave and ac susceptibility measurements can be treated from a single point of view. The differences in the experimental signals are found to be due to their different frequencies.

II. CAVITY PERTURBATION CONDITIONS

Cavity perturbation was first considered by Bethe and Schwinger.²³ For a small sample placed in a resonant cavity

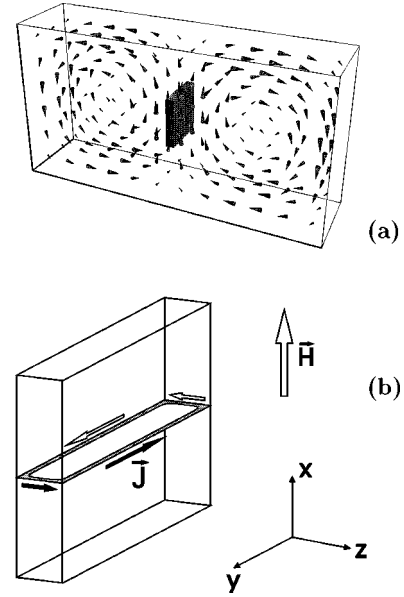


FIG. 1. (a) TE_{102} cavity with the sample in the magnetic field maximum. (b) The induced current in the sample forms a loop giving rise to a magnetic dipole moment.

and causing a weak perturbation the complex frequency shift can be expressed as²³⁻²⁷

$$\frac{\tilde{\omega} - \tilde{\omega}_0}{\tilde{\omega}} = - \frac{\int_{V_s} (\mathbf{P} \cdot \mathbf{E}_0^* + \mathbf{M} \cdot \mathbf{B}_0^*) d^3\mathbf{r}}{\int_{V_c} (\mathbf{D}_0 \cdot \mathbf{E}_0^* + \mathbf{H}_0 \cdot \mathbf{B}_0^*) d^3\mathbf{r}}, \quad (2)$$

where $\tilde{\omega}_0$ is the complex frequency of the empty cavity and $\tilde{\omega} = \tilde{\omega}_0 + \Delta\tilde{\omega}$ is the perturbed complex frequency. V_s and V_c are the volumes of the sample and cavity, respectively. \mathbf{E}_0 , \mathbf{D}_0 , \mathbf{H}_0 , and \mathbf{B}_0 are the fields of a mode in the empty cavity. \mathbf{P} and \mathbf{M} are the polarization and magnetization, respectively, induced in the sample. If the Q factor is much larger than unity, the complex frequency shift can be separated in real and imaginary parts as

$$\frac{\Delta\tilde{\omega}_0}{\tilde{\omega}} \approx \frac{\Delta\tilde{\omega}_0}{\omega} = \frac{\Delta f_0}{f} + i\Delta\left(\frac{1}{2Q_0}\right), \quad (3)$$

where $f_0 = \omega_0/2\pi$ and Q_0 are the frequency and Q factor, respectively, of the empty cavity.

The essential assumption for the validity of Eq. (2) is that the insertion of the sample into the cavity produces only a small difference in the overall geometrical configuration of the fields.²⁴ This condition is readily met for dielectric and paramagnetic samples. However, for highly conductive samples one has to reconsider the perturbation conditions.

A. Sample in magnetic field maximum

Let us first consider the case of a conducting sample placed at the location of the magnetic field maximum in the cavity. To illustrate this case we show in Fig. 1(a) a TE_{102} cavity with the conducting sample in the center. The field distribution was calculated numerically using the commercially available program MAFIA.²⁸ The magnetic field around

the sample is not very much perturbed with respect to the empty cavity. Only inside the sample the field is drastically reduced due to the induced surface current. The current has the form of a loop [Fig. 1(b)], and its role is to shield the magnetic flux. Clearly, the response to the external oscillating magnetic field is the induction of a magnetic dipole.

The complex frequency shift for the magnetic case is given by the second term in Eq. (2). In the case of a paramagnetic sample with a homogeneous distribution of spins, one can simply relate the magnetization to the external field through $\mathbf{M} = \tilde{\chi}_m \mathbf{H}_0$, where $\tilde{\chi}_m$ is the susceptibility which is an intrinsic parameter of the material and does not depend on the sample dimensions. We assume that the sample is small so that the cavity mode $\mathbf{H}_0(\mathbf{r})$ does not vary much over the sample volume, and we can take it as a uniform imposed field \mathbf{H}_0 throughout the sample. The magnetization \mathbf{M} is then also uniform. For the moment we neglect the eventual demagnetizing effects. The problem is how to treat a conductor which is free of spin magnetization. It can still be considered as a magnetic material in ac magnetic fields if the induced shielding current is interpreted as the equivalent of a bound magnetization current. In this case, however, the flux density \mathbf{B} in the sample is not uniform due to the skin effect, and we must obey

$$\mathbf{B}(\mathbf{r}) = \mu_0[\mathbf{H}_0 + \mathbf{M}(\mathbf{r})], \quad (4)$$

i.e., the magnetization must also be space dependent. This magnetization is due to the induced macroscopic current which itself decays from the surface into the bulk. If we still relate formally this magnetization to the uniform imposed field \mathbf{H}_0 in the sample, we can formally write

$$\mathbf{M}(\mathbf{r}) = \tilde{\chi}_m(\mathbf{r})\mathbf{H}_0, \quad (5)$$

where $\tilde{\chi}_m(\mathbf{r})$ is introduced as an effective magnetic susceptibility of the conducting sample in an ac magnetic field. It turns out that the conducting sample in an ac magnetic field appears as an inhomogeneous magnetic material. The inhomogeneity depends on the skin depth which may vary with temperature. Under these conditions the second integral in Eq. (2) can be formally applied to a conducting sample. It yields the complex frequency shift due to the ac magnetic field

$$\begin{aligned} \left(\frac{\Delta\tilde{\omega}_0}{\omega}\right)_m &= -\frac{1}{W_c}\mathbf{B}_0^* \cdot \int_{V_s}\mathbf{M}(\mathbf{r})d^3\mathbf{r} \\ &= -\tilde{\chi}_m\frac{\mathbf{H}_0 \cdot \mathbf{B}_0^* V_s}{W_c} = -\tilde{\chi}_m\frac{W_s}{W_c}, \end{aligned} \quad (6)$$

where W_c is the denominator in Eq. (2). We have introduced $\tilde{\chi}_m$ as the space averaged complex magnetic susceptibility of the conducting sample in an ac magnetic field. Obviously, $\tilde{\chi}_m$ is not an intrinsic property of the material since it depends not only on the conductivity but also on the sample dimensions. In Eq. (6), V_s is the sample volume and $W_s = \mathbf{H}_0 \cdot \mathbf{B}_0^* V_s$ is the energy of the cavity fields which would be contained in V_s if the sample were not there. The ratio W_s/W_c is the filling factor.

Clearly, for paramagnetic samples one can replace $\tilde{\chi}_m$ in Eq. (6) by the intrinsic $\tilde{\chi}_m$ due to spins. Thus, Eq. (6) shows that for paramagnetic samples cavity perturbation measurements yield the same kind of information as ac susceptibility measurements; only the frequency is typically higher in cavity measurements. For a conducting sample, $\tilde{\chi}_m$ is not of primary interest since it is not intrinsic. The interesting quantity is the conductivity, and we have yet to show how it can be obtained from the cavity perturbation measurement. This task will be postponed to later sections.

At this point we have to reexamine the validity of the weak perturbation assumption when a highly conducting sample is inserted in an empty cavity. To this end it is useful to express the shift given by Eq. (6) in an equivalent form with two contributions. If \mathbf{M} is taken from Eq. (4) and inserted in the integral in Eq. (6), one obtains

$$\left(\frac{\Delta\tilde{\omega}_0}{\omega}\right)_m = \frac{\mathbf{H}_0 \cdot \mathbf{B}_0^* V_s}{W_c} - \frac{1}{W_c}\mathbf{H}_0^* \cdot \int_{V_s}\mathbf{B}(\mathbf{r})d^3\mathbf{r}. \quad (7)$$

If the sample is a perfect conductor there is no penetration of the ac magnetic flux into the sample, so that $\mathbf{B} = 0$ in Eq. (7). This means that the first term in Eq. (7) gives the complex frequency shift relative to the empty cavity caused by introducing a sample which is a perfect conductor. Note that a perfect conductor yields a full diamagnetic response in an ac magnetic field, i.e., $\tilde{\chi}_m = -1$, so that Eq. (6) becomes equal to the first term in Eq. (7). The second term in Eq. (7) can then be interpreted as the complex frequency shift caused by a normal conductor sample relative to the cavity with a perfect conductor sample of the same size. This can be rationalized if we imagine that a perfect conductor acquires some finite conductivity, so that the field partially penetrates into the sample and the total shift relative to the empty cavity is reduced. This second shift term is

$$\frac{1}{W_c}\mathbf{H}_0^* \cdot \int_{V_s}\mathbf{B}(\mathbf{r})d^3\mathbf{r} = \tilde{\mu}_r\frac{\mathbf{H}_0 \cdot \mathbf{B}_0^* V_s}{W_c}, \quad (8)$$

where we introduced the space averaged complex relative permeability $\tilde{\mu}_r$ of the conducting sample in an ac magnetic field. Obviously, we have $\tilde{\mu}_r = 1 + \tilde{\chi}_m$. Note that the total shift in Eq. (6) is a measure of the induced current in the sample and therefore yields the averaged magnetization or $\tilde{\chi}_m$. In contrast, the shift in Eq. (8) is a measure of magnetic flux penetration into the sample and, hence, yields $\tilde{\mu}_r$.

In the case of paramagnetic samples the field \mathbf{B} in the sample is only slightly different from \mathbf{B}_0 , so that Eq. (7) yields a small difference of two large terms. In such a case the decomposition in Eq. (7) is useless, and Eq. (6) can better depict the small perturbation of the empty cavity. On the contrary, in conducting samples the field \mathbf{B} is significantly reduced with respect to \mathbf{B}_0 due to the induced shielding current. Therefore, the second term in Eq. (7) becomes much smaller than the first, and the total frequency shift is large. This implies also that the introduction of a conducting sample cannot be treated as a small perturbation on the empty cavity.

In order to restore the condition of weak perturbation, we propose to change the conventional approach in the perturbation treatment so that, instead of the empty cavity, we consider the cavity with a perfect conductor sample inside as the unperturbed system with the complex frequency $\tilde{\omega}_p$. Let us denote the new unperturbed field by $\mathbf{H}_p(\mathbf{r})$. This field must be tangential at the surface of the perfect conductor sample. Obviously, it is not homogeneous for a general shape of the sample and one could not take it out of the integral as we did with \mathbf{H}_0 in Eq. (8).

With the above considerations we obtain the complex frequency shift $\Delta\tilde{\omega}_p = \tilde{\omega} - \tilde{\omega}_p$ caused by a normal conductor relative to a perfect conductor sample in the cavity

$$\left(\frac{\Delta\tilde{\omega}_p}{\omega}\right)_m = -\frac{1}{W_{cp}} \int_{V_S} \mathbf{H}_p^*(\mathbf{r}) \cdot \mathbf{B}(\mathbf{r}) d^3\mathbf{r}, \quad (9)$$

where W_{cp} is the energy calculated with the new unperturbed fields.

It is important to note that Eq. (9) has been deduced using the concept usually applied to magnetic materials, i.e., the materials which develop magnetization in an external field as in Eq. (4). This means that the current induced in the conducting sample is treated as a bound current and not as a free current. Therefore, the fields used in Eq. (9) must be the solution of the Maxwell equations in such a medium. In the calculations of $\mathbf{H}_p(\mathbf{r})$ inside the sample we can take for the boundary conditions the value of $\mathbf{H}_p(\mathbf{r}_s)$ on the surface since it can be considered as an imposed field. If the penetration of $\mathbf{B}(\mathbf{r})$ into the nonperfect conductor sample is small we have the condition of small perturbation, which implies that for the tangential component of the perturbed magnetic field we set $\mathbf{H}_t(\mathbf{r}_s) \approx \mathbf{H}_p(\mathbf{r}_s)$ on the sample surface, and this serves also as the boundary condition for the calculation of $\mathbf{B}(\mathbf{r})$ in the sample. If, however, the penetration of $\mathbf{B}(\mathbf{r})$ into the nonperfect conductor sample becomes significant, the perturbed field $\mathbf{H}(\mathbf{r})$ approaches the empty cavity field \mathbf{H}_0 . Hence, for samples in which $\mathbf{H}_p(\mathbf{r})$ is much larger than \mathbf{H}_0 , the boundary conditions for the calculation of $\mathbf{B}(\mathbf{r})$ will change appreciably with the penetration. The calculation of $\mathbf{B}(\mathbf{r})$ inside the sample could also be done numerically from a self-consistent integrodifferential equation which includes the demagnetizing effects in ac magnetic fields.²⁹

In the special case of ellipsoidal samples with one of the axes along the applied field \mathbf{H}_0 , one obtains a homogeneous \mathbf{H} inside a lossless magnetic sample²⁵

$$\mathbf{H} = \frac{\mathbf{H}_0}{1 + (\mu_r - 1)N_m}, \quad (10)$$

where μ_r is the relative permeability of the magnetic material and $N_m \leq 1$ is the demagnetizing factor.³⁰ As stated above, a perfect conductor sample in an ac magnetic field can be considered as a perfect diamagnet ($\mu_r = 0$). Hence, one obtains $\mathbf{H}_p = \mathbf{H}_0 / (1 - N_m)$. This homogeneous field can be taken out of the integral in Eq. (9). For a nonperfect conductor there is a penetration of $\mathbf{B}(\mathbf{r})$ into the sample so that it acts as a nonperfect diamagnet. In the case of a small penetration of $\mathbf{B}(\mathbf{r})$ into the sample we may set for the equivalent diamagnet $\mu_r \ll 1$. If $\mu_r N_m \ll (1 - N_m)$, one obtains from Eq. (10) the field $\mathbf{H} \approx \mathbf{H}_0 / (1 - N_m) = \mathbf{H}_p$, which

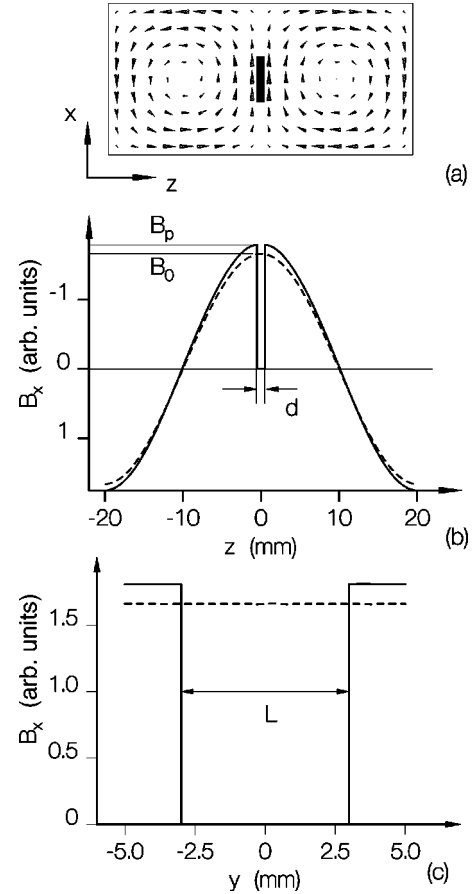


FIG. 2. (a) A cut in the xz plane through the center of the cavity and sample as presented in Fig. 1(a). The lines of the magnetic field are shown. (b) The profile of the magnetic field component B_x along the z axis through the center of the cavity and sample. (c) The profile of the magnetic field component B_x along the y axis through the center of the cavity and sample. The dashed lines in (b) and (c) show the empty cavity fields, while the solid lines are for the perfect conductor sample in place.

can be used for the calculation of $\mathbf{B}(\mathbf{r})$. For the sample which is very thin in the direction of the external field, one may have $N_m \approx 1$, so that $\mu_r N_m \gg (1 - N_m)$ and $\mathbf{H} \approx \mathbf{H}_0 / \mu_r$ which is smaller than \mathbf{H}_p for the same sample shape. When the penetration of $\mathbf{B}(\mathbf{r})$ into the sample becomes large, we have to set $\mu_r \approx 1$ and obtain $\mathbf{H} \approx \mathbf{H}_0$. Thus, in general, the boundary conditions for the calculation of $\mathbf{B}(\mathbf{r})$ may change with the perturbation, which in its turn changes with the conductivity. Only for samples elongated in the direction of the magnetic field ($N_m \approx 0$), one has $\mathbf{H} \approx \mathbf{H}_0$ regardless of the penetration of $\mathbf{B}(\mathbf{r})$. For illustration Fig. 2(a) shows the magnetic field in the xz -plane through the center of the cavity and sample, while in Figs. 2(b) and 2(c) we show the profiles of B_x along the z axis and y axis through the center of the cavity with and without the perfect conductor sample. The profiles were obtained numerically by the commercial program MAFIA.²⁸ The empty cavity field \mathbf{B}_0 is shown by a dashed line. In the case of a perfect conductor the profile shows $\mathbf{B} = 0$ inside the sample and an increased $\mathbf{B}_p(\mathbf{r})$ at the sample surface. This field takes the role of the new unperturbed state.

The above redefined perturbation approach is more suitable to describe real experiments in which a conducting

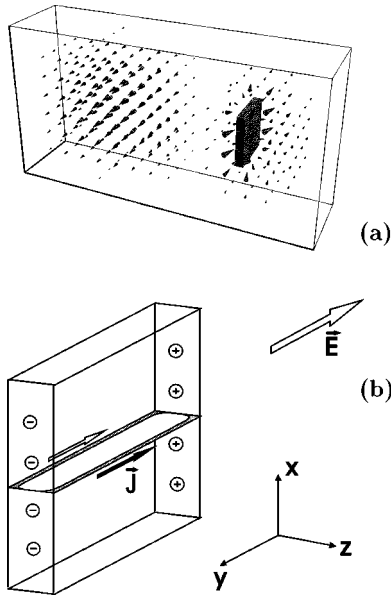


FIG. 3. (a) TE_{102} cavity with the sample in the electric field maximum. (b) The induced current in the sample forms an electric dipole.

sample of a given size is placed in the cavity and the temperature is varied. The measured frequency shifts are relative and could be given a constant offset so that data points extrapolate to zero when the conductivity increases towards infinity.

Finally, one may comment on the complex frequency shift from yet another viewpoint. The ac field $\mathbf{B}(\mathbf{r})$ stored in the sample will have a phase shift with respect to $\mathbf{H}_p(\mathbf{r})$. The integral of the in-phase component in Eq. (9) yields the field energy stored in the sample and, hence, the real frequency shift $(\Delta f_p/f)_m$. The out-of-phase component is due to dissipation, and its integral yields $\Delta(1/2Q_p)_m$.

B. Sample in electric field maximum

The case of placing a conducting sample in the electric field maximum is more complicated. In Fig. 3(a) we show the conducting sample at the position where the electric field is maximum in the empty TE_{102} cavity. The electric field was calculated by MAFIA. The electric field near the conducting sample is profoundly changed with respect to the empty cavity field at this position. The sample acts as a partial short cut for the electric field lines between the two walls of the cavity. The charges are accumulated on the rear and front sides of the sample by the surface current which flows like in an oscillating electric dipole antenna [Fig. 3(b)]. In the case of a perfect conductor, the accumulated charges compensate completely the cavity field inside the sample. The outside field is strictly perpendicular to the surface of the perfect conductor sample. It is stronger at the rear and front sides of the sample in Fig. 3 and decreases on the lateral sides. At some surface line it vanishes as the surface charges change sign. If the sample is a nonperfect conductor one finds a nonvanishing tangential ac electric field at the lateral sides of the sample. Its strength changes with the conductivity of the sample. In contrast, the electric field at the rear and front sides of the sample practically does not change with conduc-

tivity. Namely, as long as $|\tilde{\sigma}| \gg \epsilon_0 \omega$ the sample effectively retains its role as a partial short cut for the electric field lines between the cavity walls, and the change of the charge density on the rear and front sides of the sample is negligible.³¹

The complex frequency shift with respect to the empty cavity is given by Eq. (2) in which \mathbf{E}_0 stands for the empty cavity field. The perturbation can be considered to be weak if the electric field on the sample surface is not much different from \mathbf{E}_0 . With weak dielectric samples this requirement is well satisfied and Eq. (2) yields accurately the small complex frequency shift with respect to the empty cavity. For conducting samples the approximation is very poor and the shift given by Eq. (2) with \mathbf{E}_0 is incorrect. Nevertheless, we continue for the moment with Eq. (2).

The polarization \mathbf{P} is due to microscopic dipoles in the case of dielectrics and related to the internal field \mathbf{E} by $\mathbf{P} = \tilde{\chi}_e \epsilon_0 \mathbf{E}$, where $\tilde{\chi}_e$ is the complex electric susceptibility. When this relation is used for the complex frequency shift given by Eq. (2), one obtains

$$\left(\frac{\Delta \tilde{\omega}_0}{\omega} \right)_e = - \frac{1}{W_c} \mathbf{E}_0^* \cdot \int_{V_s} \mathbf{P}(\mathbf{r}) d^3 \mathbf{r} = - \tilde{\chi}_e \frac{\mathbf{D}_0^* \langle \mathbf{E}(\mathbf{r}) \rangle_r V_s}{W_c}, \quad (11)$$

where $\langle \mathbf{E}(\mathbf{r}) \rangle_r$ is the average electric field in the sample. In the case of weak dielectrics there is an almost complete field penetration so that $\langle \mathbf{E}(\mathbf{r}) \rangle_r \approx \mathbf{E}_0$, and the complex frequency shift yields the intrinsic susceptibility $\tilde{\chi}_e$ multiplied by a constant factor (filling factor W_s/W_c) which can be determined by a calibration experiment.

The problem is how to adapt the above perturbation treatment to conducting samples. We may start by considering a relatively strong dielectric sample. It is expected to cause a large frequency shift with respect to the empty cavity, so that it may appear useful to follow the analogy with the magnetic case and rewrite Eq. (11) by decomposing this shift into two parts. Using $\mathbf{D}(\mathbf{r}) = \epsilon_0 \mathbf{E}(\mathbf{r}) + \mathbf{P}(\mathbf{r})$ one obtains

$$\left(\frac{\Delta \tilde{\omega}_0}{\omega} \right)_e = - \frac{\mathbf{E}_0^* \cdot \mathbf{D}_0 V_s}{W_c} + \frac{1}{W_c} \mathbf{D}_0^* \cdot \int_{V_s} \mathbf{E}(\mathbf{r}) d^3 \mathbf{r}, \quad (12)$$

where we have used $\langle \mathbf{D}(\mathbf{r}) \rangle_r = \mathbf{D}_0$, i.e., we ignore for the moment a possible depolarizing effect. If the field $\mathbf{E}(\mathbf{r})$ in the dielectric is considerably reduced with respect to the field \mathbf{E}_0 , one can neglect the second term in Eq. (12). However, one should be cautious about extending this picture to the limit of a perfect dielectric. Namely, when ϵ_r increases the wavelength in the dielectric may become smaller than the sample size and internal modes are developing. In order to make an equivalent to a conducting sample one has to preserve the boundary value problem with equivalent surface charges. The wavelength of the fields in the equivalent dielectric sample must be finite and match the fields outside the sample. This is achieved if the material acquires a relative permittivity ϵ_r which increases to infinity and also a relative permeability μ_r which decreases to zero. Thus, a perfect dielectric must in this case also be a perfect diamagnet; both conditions are satisfied by the perfect conductor. The second term in Eq. (12) then vanishes and the first term

can be interpreted as a large shift which occurs when a perfect conductor is inserted into the cavity.

With the same argument as in the magnetic case we are led to choose that the unperturbed system consists of the cavity with a perfect conductor sample placed inside. The shift caused by a normal conductor relative to the new unperturbed state with complex frequency $\tilde{\omega}_p$ may be based on the second term in Eq. (12) which becomes

$$\left(\frac{\Delta\tilde{\omega}_p}{\omega}\right)_e = \frac{1}{W_{cp}} \int_{V_S} \mathbf{D}_p^*(\mathbf{r}) \cdot \mathbf{E}(\mathbf{r}) d^3\mathbf{r}, \quad (13)$$

where we have replaced \mathbf{D}_0 of the empty cavity with $\mathbf{D}_p(\mathbf{r})$. It results from \mathbf{D}_0 and the internal polarization which is equivalent to the charges built on the surface of the perfect conductor sample.

Equation (13) was obtained in analogy with Eq. (9) in the magnetic case. However, one can show that there is a missing term in Eq. (13) which in some cases may become very important. Already in the above qualitative reasoning we had to include a relative permeability of the sample. One may expect that this should entail also a magnetic contribution to the shift. Quite generally, the presence of a time-dependent $\mathbf{D}_p(\mathbf{r})$ in the sample involves also a space variation of the induced magnetic field due to the Maxwell equation $\nabla \times \mathbf{H}_p(\mathbf{r}) = i\tilde{\omega}_p \mathbf{D}_p(\mathbf{r})$. If the sample is flat perpendicular to the electric field direction the depolarizing effect is small, and one finds $\mathbf{D}_p(\mathbf{r}) \approx \mathbf{D}_0$. Hence, the space variation of the field $\mathbf{H}_p(\mathbf{r})$ is practically the same as that of $\mathbf{H}_0(\mathbf{r})$ in the empty cavity. When the sample is at the position of the electric field maximum and the sample dimensions are assumed to be much smaller than the wavelength in vacuum, the magnetic field in the sample is negligible. In this case we can neglect any magnetic field contribution to the complex frequency shift, and the expression given in Eq. (13) is sufficient. However, when the sample is elongated in the direction of the electric field the depolarizing effect is large, and $\mathbf{D}_p(\mathbf{r})$ in the sample becomes much larger than \mathbf{D}_0 so that the space variation of $\mathbf{H}_p(\mathbf{r})$ over the sample volume becomes large. When the sample becomes a nonperfect conductor there will be a nonvanishing $\mathbf{B}(\mathbf{r})$ inside which means that even in the position of the maximum electric field one has to include the magnetic contribution to the complex frequency shift. The general expression is

$$\frac{\Delta\tilde{\omega}_p}{\omega} = -\frac{1}{W_{cp}} \int_{V_S} [\mathbf{H}_p^*(\mathbf{r}) \cdot \mathbf{B}(\mathbf{r}) - \mathbf{D}_p^*(\mathbf{r}) \cdot \mathbf{E}(\mathbf{r})] d^3\mathbf{r}. \quad (14)$$

It can be applied to both magnetic and electric cases. In the former, the sample is in the node of the electric field so that $\mathbf{D}_p(\mathbf{r}) = 0$ and only the first term in Eq. (14) remains. On the contrary, in the electric field maximum both terms are present for the general sample shape. Obviously, Eq. (14) is also valid for all intermediate positions of the sample in the cavity. It represents our main result in the modification of the conventional Eq. (2) for the use with conducting samples.

One should note that the field $\mathbf{H}_p(\mathbf{r})$ has different functional forms for the sample in the magnetic and electric field maxima. In the former, the field $\mathbf{H}_p(\mathbf{r})$ is uniform throughout an ellipsoidal sample. It can be considered as the field im-

posed by the magnetic field in the cavity, modified eventually by the demagnetizing effect as described above. For the sample in the electric field maximum the field $\mathbf{H}_p(\mathbf{r})$ changes throughout the sample having a node in the center of the sample. This field is not imposed by the magnetic field in the cavity and does not depend on the demagnetizing effect. It is induced through the oscillating $\mathbf{D}_p(\mathbf{r})$ in the sample and depends on eventual depolarizing effects. When the sample becomes a nonperfect conductor the field $\mathbf{D}(\mathbf{r})$ inside the sample is not much changed with respect to $\mathbf{D}_p(\mathbf{r})$ as long as $|\tilde{\sigma}| \gg \epsilon_0\omega$, i.e., as long as the sample acts as an effective short cut for the electric field lines and retains practically the same accumulation of the charges on the surface. It follows from this consideration that the induced magnetic field $\mathbf{H}(\mathbf{r})$ is practically unchanged with respect to $\mathbf{H}_p(\mathbf{r})$, regardless of the penetration of $\mathbf{B}(\mathbf{r})$ into the sample. Thus, we find that for the sample in the electric field maximum the field $\mathbf{D}_p(\mathbf{r}_s)$ or $\mathbf{H}_p(\mathbf{r}_s)$ on the surface of the sample serves as the boundary condition for the calculation of $\mathbf{E}(\mathbf{r})$ and $\mathbf{B}(\mathbf{r})$. The exception to this rule is the case of a very strong depolarizing effect which will be discussed below. The calculation of the fields can be done by a self-consistent method using an integrodifferential equation in analogy to the magnetic case.²⁹

For a general shape of a conducting sample the accumulated charges on the surface will have a distribution for which the equivalent dielectric should be inhomogeneous, i.e., its relative permittivity should be space dependent $\epsilon_r(\mathbf{r})$. Ellipsoidal samples are special cases in which the distribution of charges is such that the fields in the equivalent dielectric are uniform and one can use ϵ_r as a constant quantity.

For ellipsoidal samples in the electric field one finds a homogeneous field \mathbf{D} inside a lossless dielectric sample³²

$$\mathbf{D} = \frac{\epsilon_r}{1 + (\epsilon_r - 1)N_e} \mathbf{D}_0, \quad (15)$$

where ϵ_r is the relative permittivity of the dielectric material and $N_e \leq 1$ is the depolarizing factor. A perfect conductor in an ac electric field acts equivalently to a perfect dielectric ($\epsilon_r \rightarrow \infty$). Hence, we have $\mathbf{D}_p = \mathbf{D}_0/N_e$. Obviously, this does not mean that the real permittivity of the perfect conductor is infinite but only that the perfect conductor represents the same boundary value problem as the perfect dielectric. A nonperfect conductor still acts equivalently to a very strong dielectric ($\epsilon_r \gg 1$). Again, we imply the equivalent boundary value problem. If N_e is not too small so that $\epsilon_r N_e \gg 1$, one obtains $\mathbf{D} \approx \mathbf{D}_p$. Only for samples very thin perpendicular to the field direction, for which N_e is so small that $\epsilon_r N_e \ll 1$, one finds $\mathbf{D} = \epsilon_r \mathbf{D}_0$ which is smaller than \mathbf{D}_p for the same sample shape.

For thin films one can achieve practically full penetration so that the field $\mathbf{E}(\mathbf{r})$ becomes uniform throughout the sample. For the equivalent dielectric one may set the relative permittivity as a real and homogeneous quantity $\epsilon_r \rightarrow |\tilde{\sigma}|/\epsilon_0\omega$. This will be used later in this paper.

In Fig. 4(a) we show the electric field in the yz plane through the center of the cavity and the sample located as in Fig. 3. Figure 4(b) shows the results of MAFIA for the profile of E_y along the z axis through the center of the cavity with and without the sample. At the lateral surface of the perfect conductor sample the field E_y must vanish. If the sample is a

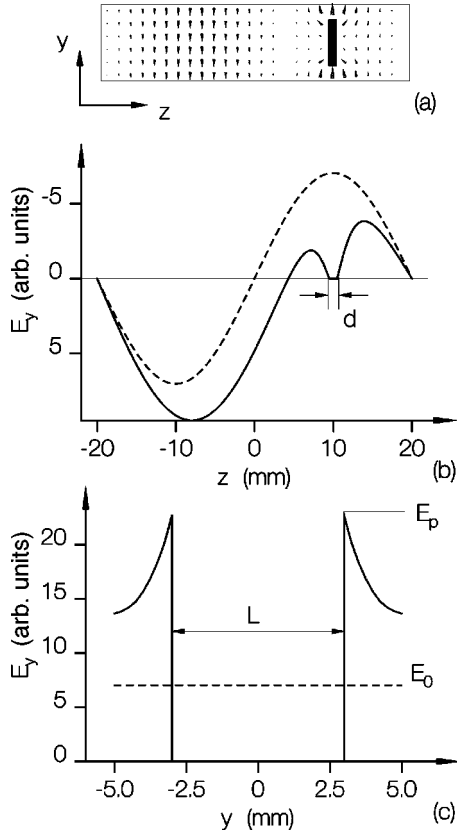


FIG. 4. (a) A cut in the yz plane through the center of the cavity and sample as presented in Fig. 3. The lines of the electric field are shown. (b) The profile of the electric field component E_y along the z axis through the center of the cavity and sample. (c) The profile of the electric field component E_y along the y axis through the center of the sample. The dashed lines in (b) and (c) show the empty cavity fields, while the solid lines are for the perfect conductor sample in place.

nonperfect conductor this lateral field will not vanish but will change with conductivity. Figure 4(c) shows the profiles of E_y along the y direction through the center of the perfect conductor sample in Fig. 3. Also shown is the profile of the field in the empty cavity. One can observe a large increase of the field E_p at the front and rear sides of the sample with respect to the empty cavity value E_0 . This field does not change much when the sample becomes a nonperfect conductor.

III. RELATION TO POYNTING VECTOR AND SURFACE IMPEDANCE

In the preceding section we started from Eq. (2) which was derived by treating the perturbation of an empty cavity by a weak dielectric or paramagnetic sample.^{23–27} Subsequently, we demonstrated the convenience of introducing a new unperturbed state for highly conducting samples. It is also possible to use the general cavity perturbation approach, but starting from the cavity plus the perfect conductor sample as the unperturbed state and calculating the perturbation caused by a finite conductivity of the sample. The complex frequency shift is found to be (see the Appendix)

$$\frac{\Delta \tilde{\omega}_p}{\omega} = \frac{i}{\omega W_{cp}} \oint_S [\mathbf{E}(\mathbf{r}_s) \times \mathbf{H}_p^*(\mathbf{r}_s)] \cdot \mathbf{n}(\mathbf{r}_s) ds, \quad (16)$$

where the integration is over the sample surface. $\mathbf{n}(\mathbf{r}_s)$ is the unit vector normal to the surface at various positions \mathbf{r}_s on the surface and pointing into the sample. The fields are taken on the outer side of the sample surface. Note that the vector product of the fields in Eq. (16) is not the Poynting vector since $\mathbf{E}(\mathbf{r}_s)$ is the perturbed field while $\mathbf{H}_p(\mathbf{r}_s)$ is the unperturbed field. Equation (16) holds regardless of the position of the sample in the electric or magnetic field in the cavity. Namely, even when the perfect conductor sample is placed in the position of the electric field maximum, the induced surface current gives rise to a tangential magnetic field $\mathbf{H}_p(\mathbf{r}_s)$ at the surface. The electric field $\mathbf{E}_p(\mathbf{r}_s)$ is perpendicular to the surface of the perfect conductor. When the sample is not a perfect conductor the field $\mathbf{E}(\mathbf{r}_s)$ acquires some tangential component, and Eq. (16) yields the complex frequency shift.

Now we have two choices for the interpretation of the properties of conducting samples. The first is that we treat the conductor as a magnetic and dielectric material as in the previous section. In that case the induced current is interpreted as a bound magnetization current if it makes loops or as a polarization current if it gives rise to surface charges. For a general position of the sample in the cavity both components of the current are present with appropriate weighting factors. In this picture we have the continuity of the tangential components of $\mathbf{E}(\mathbf{r})$ and $\mathbf{H}_p(\mathbf{r})$ across the surface of the sample so that we can apply the divergence theorem

$$\begin{aligned} & \oint_S [\mathbf{E}(\mathbf{r}_s) \times \mathbf{H}_p^*(\mathbf{r}_s)] \cdot \mathbf{n}(\mathbf{r}_s) ds \\ &= - \int_{V_S} \nabla \cdot [\mathbf{E}(\mathbf{r}) \times \mathbf{H}_p^*(\mathbf{r})] d^3 \mathbf{r} \\ &= - \int_{V_S} \mathbf{H}_p^*(\mathbf{r}) \cdot [\nabla \times \mathbf{E}(\mathbf{r})] d^3 \mathbf{r} \\ & \quad + \int_{V_S} \mathbf{E}(\mathbf{r}) \cdot [\nabla \times \mathbf{H}_p^*(\mathbf{r})] d^3 \mathbf{r}. \end{aligned} \quad (17)$$

We can use the Maxwell equations $\nabla \times \mathbf{E}(\mathbf{r}) = -i\tilde{\omega}\mathbf{B}(\mathbf{r})$ and $\nabla \times \mathbf{H}_p(\mathbf{r}) = i\tilde{\omega}_p\mathbf{D}_p(\mathbf{r})$ in the integrals of Eq. (17) and see that the complex frequency shift in Eq. (16) is equivalent to Eq. (14) derived in the previous section. We have to use the approximation $\tilde{\omega}_p \approx \tilde{\omega} \approx \omega$ which is valid for high Q factors and small frequency shifts.

The other choice is to consider the conducting sample as a nonmagnetic and nondielectric material. The induced current in the sample is then treated as free current density $\mathbf{J}(\mathbf{r})$. In this picture the perfect conductor has a free surface current density $\mathbf{J}_s = \mathbf{J}_p \delta(\mathbf{r} - \mathbf{r}_s)$, so that the field $\mathbf{H}_p(\mathbf{r}_s)$ on the outer side of the sample surface makes a jump to zero at the inner side of the surface. Therefore, the divergence theorem cannot be applied with the field $\mathbf{H}_p(\mathbf{r})$. The problem can be solved in the cases when demagnetizing and depolarizing effects are not extremely strong. As explained in the previous section the perturbed fields inside the sample are not much changed with respect to the unperturbed fields. The same holds outside the sample. The magnetic field on the outer side of the sample surface does not change appreciably when the sample becomes a nonperfect conductor, so that on the outer surface

of the actual sample one can replace $\mathbf{H}_p^{\text{ext}}(\mathbf{r}_s) \approx \mathbf{H}_t^{\text{ext}}(\mathbf{r}_s)$ where the subscript t denotes the tangential component of the perturbed field. This is the condition of weak perturbation in which we get the integral of the Poynting vector over the surface of the conductor sample. The tangential components of \mathbf{E} and \mathbf{H} are continuous across the surface of the sample so that we can apply the divergence theorem as in Eq. (17). However, now we have to use the Maxwell equations $\nabla \times \mathbf{E}(\mathbf{r}) = -i\tilde{\omega}\mu_0\mathbf{H}(\mathbf{r})$ and $\nabla \times \mathbf{H}(\mathbf{r}) = \mathbf{J}(\mathbf{r}) + i\tilde{\omega}\epsilon_0\mathbf{E}(\mathbf{r})$ which imply that the conductor is nonmagnetic ($\tilde{\mu}_r=1$) and nondielectric ($\tilde{\epsilon}_r=1$) but sustains an induced free current $\mathbf{J}(\mathbf{r})$. In this picture we have $\mathbf{D}(\mathbf{r}) = \epsilon_0\mathbf{E}(\mathbf{r})$ and $\mathbf{B}(\mathbf{r}) = \mu_0\mathbf{H}(\mathbf{r})$. Therefore the complex frequency shift becomes

$$\frac{\Delta\tilde{\omega}_p}{\omega} = -\frac{1}{W_{cp}} \int_{V_S} [\mu_0|\mathbf{H}(\mathbf{r})|^2 - \epsilon_0|\mathbf{E}(\mathbf{r})|^2] d^3\mathbf{r} + \frac{i}{\omega W_{cp}} \int_{V_S} \mathbf{J}^*(\mathbf{r})\mathbf{E}(\mathbf{r}) d^3\mathbf{r}. \quad (18)$$

The first integral in Eq. (18) represents the energy stored in the conductor sample and yield the real frequency shift. In a conductor the magnetic energy is much larger than the electric so that the second term in the first integral in Eq. (18) can be neglected. The second integral in Eq. (18) yields dissipation if $\mathbf{J}(\mathbf{r})$ and $\mathbf{E}(\mathbf{r})$ are in phase, i.e., if the conductivity is real. For a complex conductivity there is a phase shift between $\mathbf{J}(\mathbf{r})$ and $\mathbf{E}(\mathbf{r})$ and the last term in Eq. (18) yields also a contribution to the real frequency shift.³⁴

It is important to emphasize that in the cases when demagnetizing and depolarizing effects are extremely strong one finds $\mathbf{H} \ll \mathbf{H}_p$ if the magnetic field is imposed, and when the electric field is imposed $\mathbf{D} \ll \mathbf{D}_p$ which give rise to the induced magnetic field with the same condition $\mathbf{H} \ll \mathbf{H}_p$. In these cases Eq. (16) must not be replaced by the integral of the Poynting vector, and Eq. (18) does not apply. We shall come to this point later in the paper. On the other hand, Eqs. (14) and (16) are generally valid since they involve products of perturbed and unperturbed fields.

We may also have samples which are weakly conducting and, in addition, have spins and induced electric dipoles. Thus, one would have to deal with the equation $\nabla \times \mathbf{B}(\mathbf{r}) = \mu_0[\mathbf{J}(\mathbf{r}) + \nabla \times \mathbf{M}(\mathbf{r}) + i\omega\mathbf{P}(\mathbf{r}) + i\omega\epsilon_0\mathbf{E}(\mathbf{r})]$. We have to use $\mathbf{J}(\mathbf{r}) = \tilde{\sigma}\mathbf{E}(\mathbf{r})$, $\mathbf{P}(\mathbf{r}) = \tilde{\chi}_e\epsilon_0\mathbf{E}(\mathbf{r})$ and $\mathbf{M}(\mathbf{r}) = \tilde{\chi}_B\mathbf{B}(\mathbf{r})/\mu_0$,³³ so that the Maxwell equation contains only $\mathbf{E}(\mathbf{r})$ and $\mathbf{B}(\mathbf{r})$. Combining it with the other Maxwell equation $\nabla \times \mathbf{E}(\mathbf{r}) = -i\omega\mathbf{B}(\mathbf{r})$ we can find the solutions for $\mathbf{E}(\mathbf{r})$ and $\mathbf{B}(\mathbf{r})$, given the appropriate boundary conditions. Using these solutions we can obtain $\mathbf{D}(\mathbf{r}) = \tilde{\epsilon}_r\epsilon_0\mathbf{E}(\mathbf{r})$ with $\tilde{\epsilon}_r = 1 + \tilde{\chi}_e$ and $\mathbf{H}(\mathbf{r}) = (1 - \tilde{\chi}_B)\mathbf{B}(\mathbf{r})/\mu_0$. The complex frequency shift is given by Eq. (18) with the first integrand given by $[\mathbf{H}^*(\mathbf{r}) \cdot \mathbf{B}(\mathbf{r}) + \mathbf{D}^*(\mathbf{r}) \cdot \mathbf{E}(\mathbf{r})]$ as calculated by the above outlined procedure. If the sample still acts as a good diamagnetic and good dielectric, the boundary conditions are the same as discussed in the preceding section. However, if $\tilde{\chi}_e < 1$, $\tilde{\chi}_B < 1$, and $|\tilde{\sigma}| < \epsilon_0\omega$, it is more appropriate to use Eq. (2) for the complex frequency shift with respect to the empty cavity.

Equation (18) is valid also for anisotropic samples. In that case the conductivity becomes a tensor $\hat{\sigma}$ and the second integrand in Eq. (18) must be written in the form $\mathbf{E}(\mathbf{r}) \cdot \hat{\sigma}^* \cdot \mathbf{E}^*(\mathbf{r})$.

In the literature one often finds that microwave measurements are related to the surface impedance. Therefore, it is useful to examine how the complex frequency shift is related to the surface impedance problem. We have already explained above in which cases one can apply the weak perturbation condition and replace the field $\mathbf{H}_p(\mathbf{r}_s)$ in Eq. (16) by the field $\mathbf{H}(\mathbf{r}_s)$ on the surface of the actual sample. Since the integral in Eq. (16) depends only on the tangential components of the fields on the surface \mathbf{E}_t and \mathbf{H}_t , one can also make use of the surface impedance relation^{25,26}

$$\mathbf{n} \times \mathbf{E}_t(\mathbf{r}_s) = \tilde{Z}_s(\mathbf{r}_s)\mathbf{H}_t(\mathbf{r}_s). \quad (19)$$

The field \mathbf{E}_t can be formally represented as the sum of incident and reflected waves with the ratio^{25,26}

$$\frac{\tilde{E}_r}{\tilde{E}_i} = \frac{\tilde{Z}_s - Z_0}{\tilde{Z}_s + Z_0}, \quad (20)$$

where Z_0 is the impedance of the vacuum. In Eq. (20) the polarizations of the fields $\mathbf{E}_i = \mathbf{e}_i\tilde{E}_i$ and $\mathbf{E}_r = \mathbf{e}_r\tilde{E}_r$ are taken to be equal, $\mathbf{e}_i = \mathbf{e}_r$, and the complex amplitudes contain the phase information. On the surface of a perfect conductor $\tilde{Z} = 0$, so that $\tilde{E}_r = -\tilde{E}_i$, i.e., the reflected field is equal in amplitude and shifted in phase by π with respect to the incident wave so that the total field on the surface \tilde{E}_t vanishes. For a nonperfect conductor Eq. (20) yields

$$Z_0(\tilde{E}_i + \tilde{E}_r) = \tilde{Z}_s(\tilde{E}_i - \tilde{E}_r). \quad (21)$$

Noting that $\tilde{E}_i - \tilde{E}_r = Z_0(\tilde{H}_i + \tilde{H}_r)$ one obtains

$$\tilde{Z}_s = \frac{\tilde{E}_t}{\tilde{H}_t}, \quad (22)$$

which means that \tilde{Z}_s in Eq. (20) is determined by the ratio of the total fields at the surface of the sample as in Eq. (19). For the samples whose thickness is much larger than the penetration depth Eq. (22) yields the intrinsic impedance which depends on the material parameter $\tilde{\sigma}$ but not on the sample thickness [cf. Eq.(1)]. For thin samples the field \mathbf{E}_t on the surface will depend also on the sample dimensions so that the surface impedance given by Eq. (22) becomes different from the intrinsic one. It determines the reflection in Eq. (20) and the complex frequency shift in Eq. (16) which is measured in the experiments. One can introduce the quantity $\tilde{Z}_s(\mathbf{r}_s)$ as the local surface impedance which determines the ratio of the reflected and incident waves on that position of the surface. The complex frequency shift is then given by

$$\frac{\Delta\tilde{\omega}_p}{\omega} = \frac{i}{\omega W_{cp}} \oint_S \tilde{Z}_s(\mathbf{r}_s) |\mathbf{H}_t(\mathbf{r}_s)|^2 ds. \quad (23)$$

Again, this expression does not apply in the cases of extremely strong demagnetizing and depolarizing effects.

We have to remark at this point that the present case of a sample placed in a cavity is different from the cases in which the thin film sample replaces a part of the cavity walls.^{4,5} In our case the standing wave in the cavity imposes some $\mathbf{H}_t(\mathbf{r})$ on all sides of the sample, and we have a resultant $\mathbf{E}_t(\mathbf{r})$ on the surface due to the material parameter $\tilde{\sigma}$ and the sample geometry. On the contrary when the thin film sample makes a part of the cavity walls we have a transmission of radiation out of the cavity. The field $\mathbf{H}_t(\mathbf{r})$ on the outer surface of the thin film is not known and Eq. (16) loses practical significance. In such cases it is more appropriate to calculate the surface impedance on the inner surface of the thin film by impedance transformation theory.^{4,5,7}

IV. SOLUTIONS FOR SLAB GEOMETRY

A. Magnetic field maximum

Let us assume that the sample shape can be approximated by the slab geometry which describes well most single crystals and thin films of high- T_c superconductors. We consider the sample in the cavity at the position of the magnetic field maximum and oriented with its plane along the field so that the demagnetizing effect is negligible. The magnetic field at the sample surface is denoted by $H_{\parallel m}$ where the index m is a reminder of the sample position. We take it as a real quantity so that the phases of the complex fields and current are relative to $H_{\parallel m}$. For the sake of convenience we drop the vector notation in this section.

One can show that different approaches developed in the preceding sections yield the same result for the complex frequency shift. We start with Eq. (9) which assumes that the sample is a magnetic material. The complex frequency shift becomes

$$\left(\frac{\Delta\tilde{\omega}_p}{\omega}\right)_m = -\frac{H_{\parallel m}}{W_{cp}} \int_{-L_x/2}^{L_x/2} dx \int_{-L_y/2}^{L_y/2} dy \int_{-d/2}^{d/2} \tilde{B}(z) dz, \quad (24)$$

where we have set the field $H_p(z)$ as uniform throughout the sample and equal to $H_{\parallel m}$ so that it could be taken out of the integral. This condition results from the assumption that the sample thickness is much smaller than the wavelength in the cavity. The sample has dimensions $V_s = L_x L_y d$, and we assumed $L_x, L_y \gg d$. In order to evaluate the integral in Eq. (24) we have to find the analytical expression for the flux density \tilde{B} in the sample. The Maxwell equations in the conductor lead to the differential equation³⁴

$$\left(\partial_z^2 - \frac{2i}{\tilde{\delta}^2}\right) \tilde{B}(z) = 0, \quad (25)$$

where we have adopted the time dependence of the fields with the convention $\exp(i\omega t)$. In Eq. (25), $\tilde{\delta}$ is the classical skin depth $\tilde{\delta} = (2/\mu_0\omega\tilde{\sigma})^{1/2}$. The differential equation Eq. (25) for $\tilde{B}(z)$ in a magnetic medium, in which the induced current is treated as the magnetization current, is the same as the differential equation for $\tilde{H}(z)$ in a nonmagnetic medium where $\tilde{B}(z) = \mu_0\tilde{H}(z)$, and the induced current is treated as the free current.

For the slab geometry we neglect the edge effects and take the external field at the boundary planes $z = \pm d/2$ to be uniform and parallel to those planes. Due to the continuity of $\tilde{B}(z)$ at the sample surface we must have the boundary conditions for the field $\tilde{B}(z)$ in the conductor placed in a magnetic field

$$\tilde{B}_m\left(\pm\frac{d}{2}\right) = \mu_0 H_{\parallel m}. \quad (26)$$

The boundary condition in Eq. (26) is valid regardless of the penetration of $\tilde{B}(z)$ into the sample. As explained in Sec. II this is the property of the samples elongated in the direction of the magnetic field.

The solution of Eq. (25) with the boundary conditions (26) is well known:

$$\tilde{B}_m(z) = \mu_0 H_{\parallel m} \frac{\cosh\{[(1+i)/\tilde{\delta}]z\}}{\cosh\{[(1+i)/\tilde{\delta}](d/2)\}}. \quad (27)$$

Using Eq. (27) in Eq. (24) one finds the complex frequency shift

$$\left(\frac{\Delta\tilde{\omega}_p}{\omega}\right)_m = -\frac{\mu_0 H_{\parallel m}^2 V_s}{W_{cp}} \left[\frac{\tilde{\delta}}{d} (1-i) \tanh\left(\frac{1+i}{\tilde{\delta}} \frac{d}{2}\right) \right], \quad (28)$$

where we have used $L_x L_y = V_s/d$. It is obvious that the prefactor $\mu_0 H_{\parallel m}^2 V_s / W_{cp}$ stands for the filling factor of the sample in the cavity. The rest of Eq. (28) is an expression which depends on the ratio $\tilde{\delta}/d$.

The approach in which the sample is treated as a nonmagnetic material yields the same result. As pointed out above the differential equation for $\tilde{H}(z)$ is the same as Eq. (25), and with the boundary condition given by Eq. (26) one obtains the field $\tilde{H}_m(z) = \tilde{B}_m(z)/\mu_0$ as in Eq. (27). This solution implies also the solution for the electric field in the sample

$$\tilde{E}_m(z) = \frac{\mu_0 \omega}{2} H_{\parallel m} \tilde{\delta} (1+i) \frac{\sinh\{[(1+i)/\tilde{\delta}]z\}}{\cosh\{[(1+i)/\tilde{\delta}](d/2)\}}. \quad (29)$$

The induced current density is given by

$$\tilde{J}_m(z) = H_{\parallel m} \left(\frac{1+i}{\tilde{\delta}}\right) \frac{\sinh\{[(1+i)/\tilde{\delta}]z\}}{\cosh\{[(1+i)/\tilde{\delta}](d/2)\}} \quad (30)$$

and should be treated as the free current in a nonmagnetic material. When we use Eq. (18) and neglect the integral of the electric field energy in the sample we find the result which is identical to that of Eq. (28).

It is easy to verify that one can also use Eq. (23) with the surface impedance defined by the fields on the surface. From Eq. (29) one finds

$$\tilde{Z}_{sm} = \frac{\tilde{E}_{\parallel m}}{H_{\parallel m}} = \frac{\mu_0 \omega}{2} \left[\tilde{\delta} (1+i) \tanh\left(\frac{1+i}{\tilde{\delta}} \frac{d}{2}\right) \right]. \quad (31)$$

The complex frequency shift calculated from Eq. (23) is

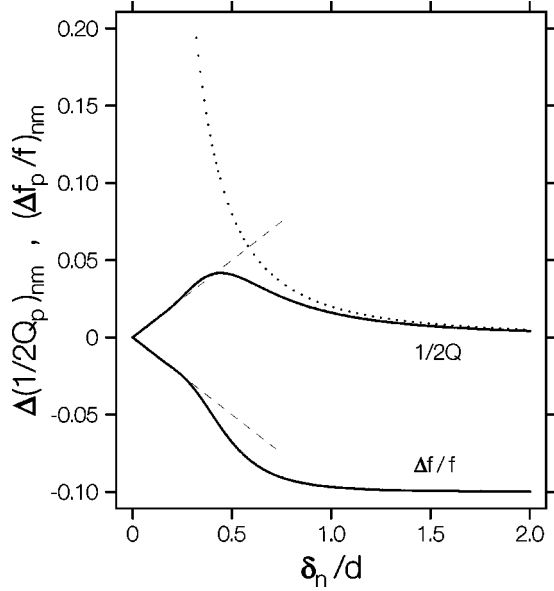


FIG. 5. Plots of $(\Delta f_p/f)_{nm}$ and $\Delta(1/2Q_p)_{nm}$ given by Eqs. (33) and (34) for a constant filling factor (chosen to be 0.1) of the sample in the magnetic field maximum in the cavity. The dashed lines indicate the linear behavior for thick samples ($\delta_n \ll d$), while the dotted line shows the asymptotic behavior $1/\delta_n^2$ for electromagnetically thin samples ($\delta_n \gg d$).

$$\left(\frac{\Delta \tilde{\omega}_p}{\omega} \right)_m = 2 \frac{\mu_0 H_{\parallel m}^2 V_s}{W_{cp}} \left(\frac{i \tilde{Z}_{sm}}{\mu_0 \omega d} \right), \quad (32)$$

which is equivalent to Eq. (28).

The above complex frequency shift can be related also to the average relative permeability $\tilde{\mu}_r$ of the sample. When Eq. (8) is specified to the slab geometry one finds that Eq. (28) can be expressed as $(\Delta \tilde{\omega}_p/\omega)_m = -(\mu_0 H_{\parallel m}^2 V_s / W_{cp}) \tilde{\mu}_r$. Thus, the real and imaginary parts of $\tilde{\mu}_r$ multiplied by the filling factor yield $(\Delta f_p/f)_m$ and $\Delta(1/2Q_p)_m$, respectively.

Equation (28) holds for both normal conductors and superconductors. In order to separate the real and imaginary parts we would have to specify whether the conductor is a normal metal with σ_n and δ_n as real quantities or a superconductor with $\tilde{\sigma}$ and $\tilde{\delta}$ as complex quantities.

For the moment we proceed with a normal metal and treat the superconducting case in a later subsection. The real and imaginary parts of Eq. (28) become

$$\left(\frac{\Delta f_p}{f} \right)_{nm} = - \frac{\mu_0 H_{\parallel m}^2 V_s}{W_{cp}} \left[\frac{\delta_n}{d} \frac{\sinh(d/\delta_n) + \sin(d/\delta_n)}{\cosh(d/\delta_n) + \cos(d/\delta_n)} \right], \quad (33)$$

$$\Delta \left(\frac{1}{2Q_p} \right)_{nm} = \frac{\mu_0 H_{\parallel m}^2 V_s}{W_{cp}} \left[\frac{\delta_n}{d} \frac{\sinh(d/\delta_n) - \sin(d/\delta_n)}{\cosh(d/\delta_n) + \cos(d/\delta_n)} \right], \quad (34)$$

where the subscript n refers to the normal conductor.

It is interesting to analyze these results. Figure 5 shows $(\Delta f_p/f)_{nm}$ and $\Delta(1/2Q_p)_{nm}$ as functions of δ_n . The sample thickness d is considered to be a constant so that the prefactors are fixed. From the experimental point of view we may say that the penetration depth is varied due to a change in the

resistivity of the metal with temperature. We may choose the sample thickness d so that at low temperatures $\delta_n \ll d$ and the sample is electromagnetically thick. Both $(\Delta f_p/f)_{nm}$ and $\Delta(1/2Q_p)_{nm}$ vary linearly with the penetration depth δ_n in this regime. When δ_n becomes comparable to half of the sample thickness d , $\Delta(1/2Q_p)_{nm}$ reaches a maximum and decreases at higher temperatures where the penetration becomes complete ($\delta_n > d$), i.e., the sample becomes electromagnetically thin. In the limit $\delta_n \gg d$, $\Delta(1/2Q_p)_{nm}$ decreases as $(1/\delta_n^2)$. It may appear puzzling that the losses represented by $\Delta(1/2Q_p)_{nm}$ decrease when the resistivity of the sample increases. In order to understand the physics of this process one has to analyze the penetrated field and current in the sample. Namely, the induced current forms a loop whose role is to shield the magnetic flux from the sample. Full penetration must imply that the shielding current has been reduced practically to zero and this in turn implies that the dissipation must vanish. The real frequency shift must saturate at $\delta_n \gg d$ since it reflects the total change of the energy stored in the sample volume.

B. Electric field maximum

Now we consider the sample of approximately slab geometry in the electric field maximum as shown in Fig. 3. The depolarizing effect may now be large, and this makes it different with respect to the magnetic case where the demagnetizing effect is negligible. In the picture of equivalent dielectric and magnetic material the complex frequency shift is given by Eq. (14). The Maxwell equation for the perfect conductor reads

$$\partial_z H_p(z) = i \omega D_p, \quad (35)$$

where we neglected the edge effects and assume that D_p is uniform throughout the sample. This also implies that the field $H_{\parallel e}$, which is induced on the surface of the sample due to the oscillating D_p , is uniform along the surface. One obtains by integration of Eq. (35) from the center of the slab to the surface

$$H_{\parallel e} = H_p \left(\frac{d}{2} \right) = i \omega D_p \frac{d}{2}. \quad (36)$$

This equation relates D_p to $H_{\parallel e}$ which can be conveniently used as the boundary condition for the calculation of other fields. It follows from Eqs. (35) and (36) that the field $H_p(z)$ has a simple linear form

$$H_p(z) = \frac{2H_{\parallel e}}{d} z. \quad (37)$$

Besides the unperturbed fields $H_p(z)$ and D_p one also needs the perturbed fields $\tilde{B}(z)$ and $\tilde{E}(z)$ for the calculation of the complex frequency shift in Eq. (14). We can use the same differential equation given in Eq. (25) but the boundary conditions have to be examined carefully. If we assume that the depolarizing factor is not too small, so that one can take $D \approx D_p$ (see Sec. II.), the field $H_{\parallel e}$ given by Eq. (36) can also be set for the perturbed field on the surface. One has

$$\tilde{B}_e\left(\frac{d}{2}\right) = -\tilde{B}_e\left(-\frac{d}{2}\right) = \mu_0 H_{\parallel e}. \quad (38)$$

The case of extremely small depolarizing factor will be discussed in the next section. The solution of Eq. (25) with the boundary conditions (38) is

$$\tilde{B}_e(z) = \mu_0 H_{\parallel e} \frac{\sinh\{[(1+i)/\tilde{\delta}]z\}}{\sinh\{[(1+i)/\tilde{\delta}](d/2)\}}, \quad (39)$$

and one finds the electric field

$$\tilde{E}_e(z) = \frac{\mu_0 \omega}{2} H_{\parallel e} \tilde{\delta} (1+i) \frac{\cosh\{[(1+i)/\tilde{\delta}]z\}}{\sinh\{[(1+i)/\tilde{\delta}](d/2)\}}. \quad (40)$$

One can now evaluate Eq. (14) and obtain

$$\left(\frac{\Delta \tilde{\omega}_p}{\omega}\right)_e = -\frac{\mu_0 H_{\parallel e}^2 V_s}{W_{cp}} \left[\frac{\tilde{\delta}}{d} (1-i) \coth\left(\frac{1+i}{\tilde{\delta}} \frac{d}{2}\right) \right]. \quad (41)$$

The prefactor $\mu_0 H_{\parallel e}^2 V_s / W_{cp}$ is the filling factor of the sample at the position of the maximum electric field in the cavity.

In the picture of a nonmagnetic and nondielectric conducting sample which sustains a free current density, one finds

$$\tilde{J}_e(z) = H_{\parallel e} \left(\frac{1+i}{\tilde{\delta}} \right) \frac{\cosh\{[(1+i)/\tilde{\delta}]z\}}{\sinh\{[(1+i)/\tilde{\delta}](d/2)\}}, \quad (42)$$

and Eq. (18) has to be used for the calculation of the complex frequency shift. The second term in Eq. (18) can be neglected and the final result is the same as in Eq. (41).

One may note that in this picture the induced boundary field $H_{\parallel e}$ has also the meaning of an equivalent surface current

$$H_{\parallel e} = \int_0^{d/2} \tilde{J}(z) dz. \quad (43)$$

This current gives rise to the accumulation of charges on the sample surface. The space averaged current density is $\bar{J} = 2H_{\parallel e}/d$ which is equivalent to $\bar{J} \equiv i\omega D$ in the picture of an equivalent dielectric sample. Therefore, \bar{J} depends on the shape of the sample through the depolarizing factor as discussed above.

Alternatively, one may use the surface impedance in the electric case obtained from Eq. (40)

$$\tilde{Z}_{se} = \frac{\tilde{E}_{\parallel e}}{H_{\parallel e}} = \frac{\mu_0 \omega}{2} \left[\tilde{\delta} (1+i) \coth\left(\frac{1+i}{\tilde{\delta}} \frac{d}{2}\right) \right] \quad (44)$$

and calculate the complex frequency shift from Eq. (23) for the slab geometry

$$\left(\frac{\Delta \tilde{\omega}_p}{\omega}\right)_e = 2 \frac{\mu_0 H_{\parallel e}^2 V_s}{W_{cp}} \left(\frac{i \tilde{Z}_{se}}{\mu_0 \omega d} \right), \quad (45)$$

which is identical to Eq. (41).

Equation (41) yields the complex frequency shift caused by a normal conductor or a superconductor relative to the

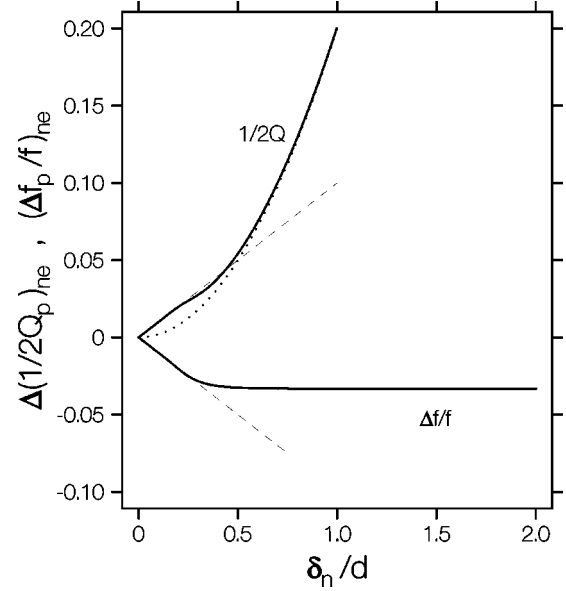


FIG. 6. Plots of $(\Delta f_p/f)_{ne}$ and $\Delta(1/2Q_p)_{ne}$ given by Eqs. (46) and (47) for a constant filling factor (chosen to be 0.1) of the sample in the electric field maximum in the cavity. The dashed lines indicate the linear behavior for thick samples ($\delta_n \ll d$), while the dotted line shows the asymptotic behavior δ_n^2 for electromagnetically thin samples ($\delta_n \gg d$).

perfect conductor. We shall first analyze the case of a normal metal and postpone the discussion of superconductors to the next subsection. With δ_n real, Eq. (41) can be separated into the real and imaginary parts

$$\left(\frac{\Delta f_p}{f}\right)_{ne} = -\frac{\mu_0 H_{\parallel e}^2 V_s}{W_{cp}} \left[\frac{\delta_n}{d} \frac{\sinh(d/\delta_n) - \sin(d/\delta_n)}{\cosh(d/\delta_n) - \cos(d/\delta_n)} \right], \quad (46)$$

$$\Delta\left(\frac{1}{2Q_p}\right)_{ne} = \frac{\mu_0 H_{\parallel e}^2 V_s}{W_{cp}} \left[\frac{\delta_n}{d} \frac{\sinh(d/\delta_n) + \sin(d/\delta_n)}{\cosh(d/\delta_n) - \cos(d/\delta_n)} \right], \quad (47)$$

where the subscript n refers to the normal conductor.

Figure 6 shows the dependence of $(\Delta f_p/f)_{ne}$ and $\Delta(1/2Q_p)_{ne}$ on the penetration depth δ_n while the sample thickness d is considered to be a constant so that the prefactor is fixed. At low temperatures where the sample is electromagnetically thick ($\delta_n \ll d$), the shifts are linear in δ_n as in the magnetic case in Fig. 5. At elevated temperatures where $\delta_n > d$, $\Delta(1/2Q_p)_{ne}$ increases nonlinearly and acquires δ_n^2 dependence in the limit $\delta_n \gg d$. This is remarkably different from the magnetic case in Fig. 5. One can explain this behavior by analyzing the induced current in the sample. In contrast to the magnetic case the current in the electric case has the same sign on both sides of the sample. When the penetration depth is increased the current does not diminish but becomes more uniform throughout the sample. Therefore, the losses then have to increase with the resistivity of the sample, i.e., with δ_n^2 . Note that the induced current in the electric case flows similar to in an antenna (Fig. 3), i.e., it does not make a loop and does not serve to shield the magnetic flux. In fact Eqs. (38),(39) show that the magnetic field changes sign when going from the left to the right side of the

sample so that there is no net magnetic flux in the sample. Hence, full penetration does not imply that the induced current vanishes. The real frequency shift must saturate for $\delta_n \gg d$ because of the same reasons as given in the magnetic case.

C. Arbitrary position

If the sample is placed at an arbitrary position between the magnetic and electric fields maxima, the boundary conditions will be a mixture of Eqs. (26) and (38). Namely, if $\tilde{B}(-d/2) \neq \tilde{B}(d/2)$ one can write the sum and difference

$$\mu_0 H_{\parallel m} = \frac{1}{2} \left[\tilde{B}\left(\frac{d}{2}\right) + \tilde{B}\left(-\frac{d}{2}\right) \right], \quad (48)$$

$$\mu_0 H_{\parallel e} = \frac{1}{2} \left[\tilde{B}\left(\frac{d}{2}\right) - \tilde{B}\left(-\frac{d}{2}\right) \right], \quad (49)$$

so that the boundary values are expressed in the form

$$\tilde{B}\left(\frac{d}{2}\right) = \mu_0 (H_{\parallel m} + H_{\parallel e}), \quad (50)$$

$$\tilde{B}\left(-\frac{d}{2}\right) = \mu_0 (H_{\parallel m} - H_{\parallel e}). \quad (51)$$

One can see that $H_{\parallel m}$ enters the boundary conditions with the form of Eq. (26) while $H_{\parallel e}$ contributes as the field in Eq. (38). Hence, one may say that $H_{\parallel m}$ and $H_{\parallel e}$ are the boundary fields induced by the magnetic and electric effects, respectively. The induced current in the sample is the superposition of the loop current [magnetic dipole, Fig. 1(b)] and antenna current [electric dipole, Fig. 3(b)]. The complex frequency shift is the superposition of the contributions from Eqs. (28) and (41). Which of the two contributions will prevail depends on the ratio of $H_{\parallel m}$ to $H_{\parallel e}$ but also on the factors involving d/δ_n as will be discussed in the following sections.

D. Superconducting samples

The ideas developed above apply also in the case of superconducting samples. The corresponding expressions for superconductors can be readily obtained with the conductivity $\tilde{\sigma}$ and penetration depth $\tilde{\delta}$ as complex quantities. One could evaluate the real and imaginary parts of the complex frequency shift. It is, however, more common to introduce the complex penetration length $\tilde{\lambda}$ through the equation

$$\frac{1+i}{\tilde{\delta}} = \frac{1}{\tilde{\lambda}}. \quad (52)$$

With this definition of $\tilde{\lambda}$, Eq. (25) takes the form of the London equation

$$\left(\partial_z^2 - \frac{1}{\tilde{\lambda}^2} \right) \tilde{B}(z) = 0. \quad (53)$$

In the normal state the real and imaginary parts of $\tilde{\lambda}$ are found from Eq. (52) to be

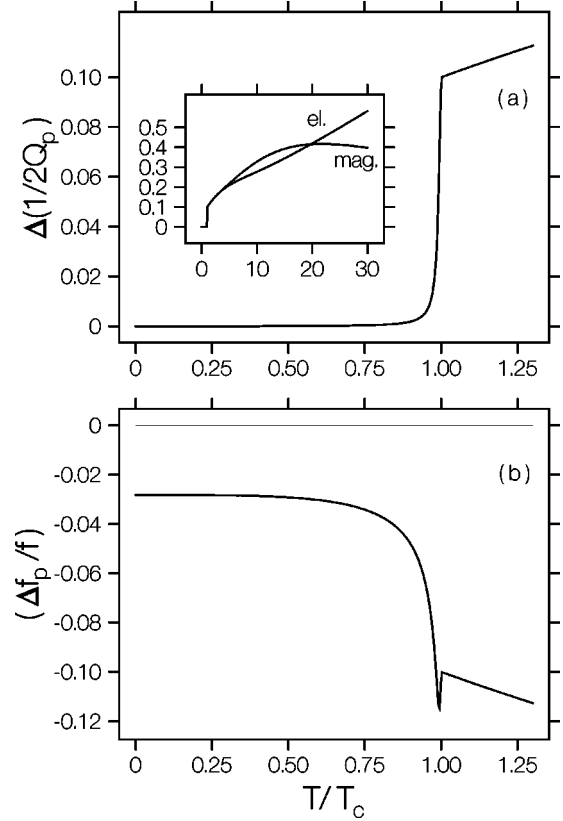


FIG. 7. (a) Calculated temperature dependences of $\Delta(1/2Q_p)_m$ and $\Delta(1/2Q_p)_e$ for a thick superconducting sample with $d = 10\delta_n(T_c)$. For other parameters see the text. The two curves overlap below T_c , and slightly above T_c , while at elevated temperatures the sample becomes electromagnetically thin and the curves separate (inset). (b) Calculated temperature dependences of $(\Delta f_p/f)_m$ and $(\Delta f_p/f)_e$ for the same sample as in (a).

$$\tilde{\lambda} = \lambda_1 - i\lambda_2 = \frac{\delta_n}{2} (1 - i), \quad (54)$$

where δ_n is real. Thus, $\lambda_1 = \lambda_2$ in the normal state. In the superconducting state with $\tilde{\sigma} = \sigma_1 - i\sigma_2$ one finds

$$\lambda_{1,2} = \sqrt{\frac{|\tilde{\sigma}| \pm \sigma_2}{2\mu_0\omega|\tilde{\sigma}|^2}}, \quad (55)$$

where plus and minus signs apply to λ_1 and λ_2 , respectively. Clearly, when the superconducting state occurs, $\sigma_2 > 0$ and λ_1 becomes larger than λ_2 . At zero temperature one should have $\sigma_1(0) = 0$ and $\sigma_2(0) = 1/\mu_0\omega\lambda_L(0)^2$ where $\lambda_L(0)$ is the zero temperature London penetration length. From Eq. (55) one finds $\lambda_1(0) = \lambda_L(0)$ and $\lambda_2(0) = 0$, i.e., $\tilde{\lambda}$ becomes real and equal to $\lambda_L(0)$ so that Eq. (53) reduces to the original London equation.

Using Eq. (52) one can express Eq. (28) for the complex frequency shift of the sample in the magnetic field maximum in an equivalent form

$$\left(\frac{\Delta\tilde{\omega}_p}{\omega} \right)_m = -2 \frac{\mu_0 H_{\parallel m}^2 V_s}{W_{cp}} \left[\frac{\tilde{\lambda}}{d} \tanh\left(\frac{d}{2\tilde{\lambda}}\right) \right]. \quad (56)$$

If the sample is a superconductor, the real and imaginary parts become

$$\left(\frac{\Delta f_p}{f}\right)_{sm} = -2 \frac{\mu_0 H_{\parallel m}^2 V_s}{W_{cp}} \left[\frac{\lambda_1/d \sinh[(\lambda_1/|\tilde{\lambda}|^2)d] + (\lambda_2/d) \sin[(\lambda_2/|\tilde{\lambda}|^2)d]}{\cosh[(\lambda_1/|\tilde{\lambda}|^2)d] + \cos[(\lambda_2/|\tilde{\lambda}|^2)d]} \right], \quad (57)$$

$$\Delta \left(\frac{1}{2Q_p}\right)_{sm} = 2 \frac{\mu_0 H_{\parallel m}^2 V_s}{W_{cp}} \left[\frac{\lambda_2/d \sinh[(\lambda_1/|\tilde{\lambda}|^2)d] - (\lambda_1/d) \sin[(\lambda_2/|\tilde{\lambda}|^2)d]}{\cosh[(\lambda_1/|\tilde{\lambda}|^2)d] + \cos[(\lambda_2/|\tilde{\lambda}|^2)d]} \right], \quad (58)$$

where the subscript s refers to the superconducting state. These expressions obviously reduce to Eqs. (33),(34) for the normal state when $\lambda_1 = \lambda_2 = \delta_n/2$. Note that the superconductor at $T=0$ is still different from a perfect conductor. For the latter $\delta_n \rightarrow 0$, while the superconductor still retains the penetration length $\lambda_L(0)$ so that there is a finite real frequency shift in Eq. (57) of the superconductor relative to the perfect conductor. There is no difference in the Q factor, i.e., $\Delta(1/2Q_p)_{sm}$ in Eq. (58) vanishes at zero temperature. The factors in the brackets in Eqs. (57) and (58) were found also by Coffey and Clem³⁵ who calculated the average relative permeability $\bar{\mu}_r$.

For the sample in the electric field maximum Eq. (41) can be given an equivalent form using $\tilde{\lambda}$ from Eq. (52)

$$\left(\frac{\Delta \tilde{\omega}_p}{\omega}\right)_e = -2 \frac{\mu_0 H_{\parallel e}^2 V_s}{W_{cp}} \left[\frac{\tilde{\lambda}}{d} \coth\left(\frac{d}{2\tilde{\lambda}}\right) \right]. \quad (59)$$

For a superconductor the real and imaginary parts are found to be

$$\left(\frac{\Delta f_p}{f}\right)_{se} = -2 \frac{\mu_0 H_{\parallel e}^2 V_s}{W_{cp}} \left[\frac{(\lambda_1/d) \sinh[(\lambda_1/|\tilde{\lambda}|^2)d] - (\lambda_2/d) \sin[(\lambda_2/|\tilde{\lambda}|^2)d]}{\cosh[(\lambda_1/|\tilde{\lambda}|^2)d] - \cos[(\lambda_2/|\tilde{\lambda}|^2)d]} \right], \quad (60)$$

$$\Delta \left(\frac{1}{2Q_p}\right)_{se} = 2 \frac{\mu_0 H_{\parallel e}^2 V_s}{W_{cp}} \left[\frac{(\lambda_2/d) \sinh[(\lambda_1/|\tilde{\lambda}|^2)d] + (\lambda_1/d) \sin[(\lambda_2/|\tilde{\lambda}|^2)d]}{\cosh[(\lambda_1/|\tilde{\lambda}|^2)d] - \cos[(\lambda_2/|\tilde{\lambda}|^2)d]} \right]. \quad (61)$$

Equations (60),(61) reduce to Eqs. (46),(47) when $\lambda_1 = \lambda_2 = \delta_n/2$. To the best of our knowledge Eqs. (59)–(61) for the superconducting sample in the microwave electric field have not been reported previously.

In order to illustrate the behavior of the shifts in superconducting samples one needs to assume a model for the temperature variations of σ_1 and σ_2 which then determine the temperature dependences of λ_1 and λ_2 . For the present purpose we assume the two fluid model in which $\sigma_1(t) = \sigma_n(T_c)t^4$ and $\sigma_2(t) = \sigma_2(0)(1-t^4)$ where $t = T/T_c$ is the reduced temperature. The value that has to be taken for $\sigma_2(0)$ depends on the London penetration length $\lambda_L(0)$ at zero temperature and the operating frequency. For $t > 1$, i.e., in the normal state, we assume a metallic behavior $\sigma_n(t) = \sigma_n(T_c)/(\alpha t + \beta)$, typical for high- T_c cuprates and set for simplicity $\alpha = 0.9$ and $\beta = 0.1$. Thus, we get the temperature dependences of $\delta_n(t)$, $\lambda_1(t)$, and $\lambda_2(t)$ relative to the value of δ_n at T_c . In what follows we use $K = [\sigma_2(0)/\sigma_n(T_c)] = 25$, which is typical at microwave frequencies.

It is interesting to analyze two choices for the sample thickness d with respect to $\delta_n(T_c)$. If we choose $d \gg \delta_n(T_c)$ the sample is electromagnetically thick at T_c . By cooling it below T_c , λ_1 and λ_2 are further reduced, so that the sample remains electromagnetically thick in the whole temperature region.

Figure 7 shows the evolution of the complex frequency shift for $d = 10\delta_n(T_c)$ in the cases when the sample is placed in the magnetic or electric field maximum. For simplicity we have taken the filling factors to be 0.1 in both cases. The

shifts in the two cases show no difference below T_c and just above T_c since the sample is electromagnetically thick in this region. For thick samples the expression in the brackets of Eqs. (57) and (60) for the frequency shift reduces to $\lambda_1(t)/d$ while the brackets for the absorption Eqs. (58) and (61) reduce to $\lambda_2(t)/d$. The surface impedances \tilde{Z}_{sm} and \tilde{Z}_{se} given by Eqs (31) and (44), respectively, are both equal to the intrinsic surface impedance \tilde{Z}_s in Eq (1). The intrinsic surface impedance can be expressed using Eq. (52) as $\tilde{Z}_s(t) = i\mu_0\omega\tilde{\lambda}(t)$, so that $R_s(t) = \mu_0\omega\lambda_2(t)$ and $X_s(t) = \mu_0\omega\lambda_1(t)$.

At temperatures much larger than T_c the differences between the magnetic and electric cases in Fig. 7 become noticeable because $\delta_n(t)$ increases to become comparable and larger than d (cf. Figs. 5 and 6).

The other choice $d \ll \delta_n(T_c)$ becomes very interesting for thin films. The sample is obviously electromagnetically thin everywhere in the normal state. For the illustration in Fig. 8 we take $d = 0.1\delta_n(T_c)$. For simplicity we assume again that the filling factors in the magnetic and electric cases are equal and set the value to 10^{-3} . This choice simply accounts for the change in V_s with respect to the previous case of the thick sample. A more elaborated approach including the consequences of the depolarizing effect will be discussed in the next section. Figure 8(a) shows that the absorption signal $\Delta(1/2Q_p)$ is much smaller in the magnetic than in the electric case. Moreover, when the signal amplitudes are compared to those of the thick sample in Fig. 7(a), one can ob-

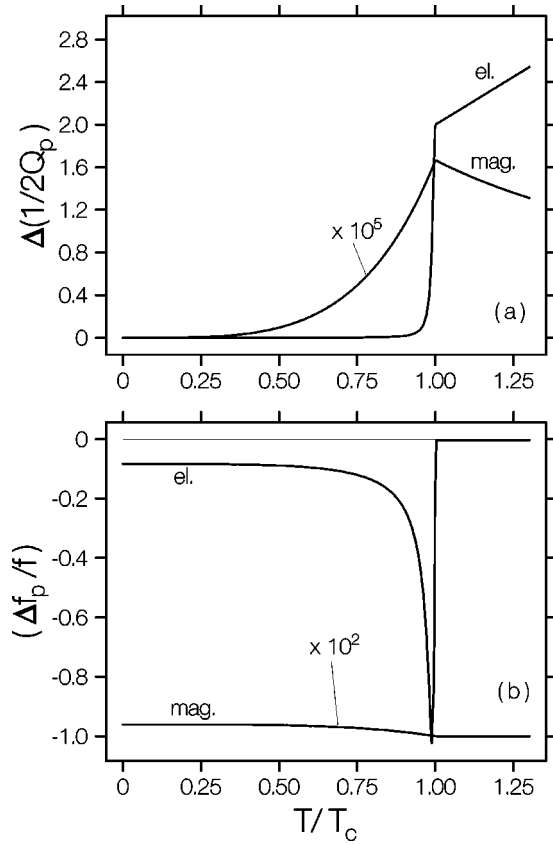


FIG. 8. (a) The same as in Fig. 7(a), but for a thin sample with $d=0.1\delta_n(T_c)$. $\Delta(1/2Q_p)_m$ is much smaller and has a much broader transition below T_c than $\Delta(1/2Q_p)_e$. (b) Calculated frequency shifts for the sample as in (a).

serve that the signal in the magnetic case is reduced much more than just because of the filling factor. In contrast, the signal amplitude in the electric case is even increased with respect to the thick sample. One also observes that in the magnetic case the superconducting transition appears broadened while it remains sharp in the electric case.

The frequency shifts shown in Fig. 8(b) are particularly interesting. In the magnetic case the amplitude of the signal is reduced with respect to the thick sample and the shape becomes very flat. At the same time the shape of the signal in the electric case changes dramatically with respect to the thick sample. The shift in the normal state becomes very small and a sharp negative peak is seen just below T_c . Its origin is in the numerator in Eq. (60) and a rapid drop of λ_2 below T_c . One may observe that the magnitude of the frequency shift at zero temperature is increased with respect to the thick sample.

The reason why the signals in the electric case grow in amplitude when the sample becomes thinner, even though the filling factor is reduced as required by V_s , can be rationalized when the expressions in the brackets of Eqs. (60) and (61) are expanded for $(d/\lambda_{1,2} \ll 1)$. One finds that these expressions increase as d^{-2} so that the signal amplitudes increase as d^{-1} . The corresponding surface impedance \tilde{Z}_{se} in Eqs. (44),(45) also increases as d^{-1} in accord with the expression given by Gittleman and Rosenblum.³⁶ At this point one may address the question of extremely thin samples. Obviously, the divergence of the signal intensities for $d \rightarrow 0$

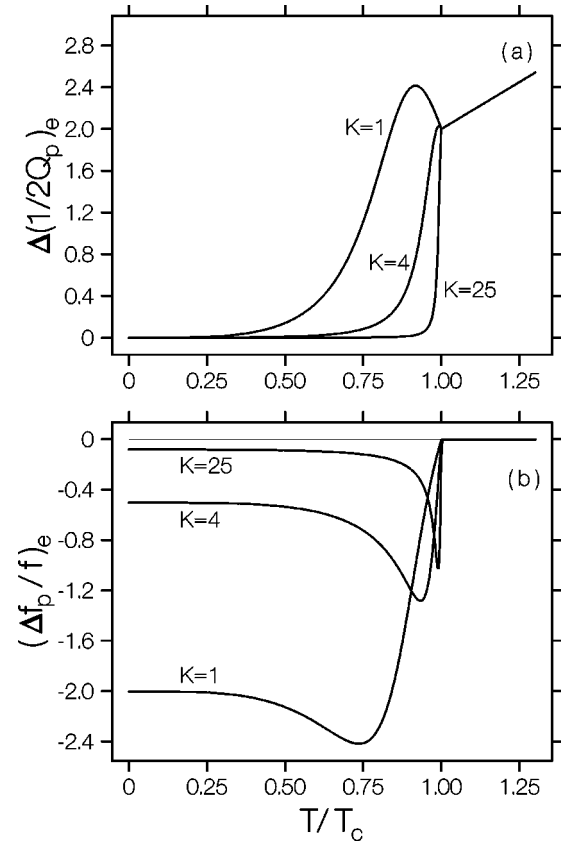


FIG. 9. Calculated temperature dependences of the absorption and frequency shift as in Fig. 8 for a thin sample in the electric field, but with $K = [\sigma_2(0)/\sigma_n(T_c)] = 1, 4, \text{ and } 25$.

could not be physical. To solve the problem one has to analyze also a more intricate dependence coming from the depolarizing effect on $H_{\parallel e}$ which will be discussed in the next section.

There is an additional feature in the signals for thin films in the electric field maximum. The calculations in Fig. 8 were made with the choice of the parameter $K = [\sigma_2(0)/\sigma_n(T_c)] = 25$ as mentioned above. It is worth noting that a very interesting behavior is obtained for smaller values of K (Fig. 9). The absorption curves broaden and develop a peak just below T_c . The negative peak in the frequency shift also broadens and the curves acquire a steplike form. These cases may become relevant for low temperature superconductors where $\sigma_n(T_c)$ is large and/or for any superconductor in experiments at elevated frequencies where $\sigma_2(0)$ is lower.

V. DISCUSSION OF THE EXPERIMENTAL CONDITIONS FOR THIN FILM SAMPLES

In a typical microwave conductivity measurement one uses a sample of given dimensions and measures the changes of f and Q as a function of temperature. If the sample is a good conductor in the whole temperature range of the experiment, the field H_{\parallel} on its surface does not change if the cavity parameters do not change with temperature. It is fixed by the dimensions of the sample and its position in the cavity. The shifts $\Delta f_p/f$ and $\Delta(1/2Q_p)$ are then functions of the penetration length $\tilde{\lambda}$ which itself is a function of temperature.

The aim of microwave measurements of superconductors is to determine the temperature dependences $\sigma_1(t)$ and $\sigma_2(t)$. The case of thick samples causes no problem in the interpretation of the experimental data, i.e., in extracting $\sigma_1(t)$ and $\sigma_2(t)$ in an unequivocal way. One uses the theoretical expression for the complex frequency shift which is the same for the position of the sample in both the magnetic and electric field maxima. A small misalignment of the sample from a desired position does not change the temperature dependence of the complex frequency shift and the analysis remains valid.

The situation is more complicated in thin films. In some of the reported experiments^{10–12} the sample was placed at the position of the magnetic field maximum in the cavity. It was oriented so that the microwave magnetic field was parallel to the plane of the film which means that the condition for a thin sample in the slab geometry was met. It was observed that the microwave absorption increased with temperature above T_c which is in contrast to the negative slope of $\Delta(1/2Q_p)_{nm}$ in Fig. 5 but agrees qualitatively with the signal $\Delta(1/2Q_p)_{ne}$ in Fig. 6. Also the observed transition below T_c was sharp as predicted for the electric case, rather than being broadened as expected for the magnetic case (cf. Fig. 8). We claim that the reported observations were due to a small misalignment of the sample from the nodal plane of the electric field. Note that in a real experiment the dielectric substrate on which the thin film is grown will displace slightly the nodal plane of the electric field from its position in the empty cavity. Therefore it becomes very unlikely to reach the exact position of the thin film in the nodal plane of the electric field.

An interesting question is how the signal amplitudes may vary when microwave measurements are carried out on ever thinner samples. In the magnetic case we must analyze Eqs. (57),(58) in the limit $d \rightarrow 0$. Since $H_{\parallel m}$ is independent of d in the slab geometry and $V_s \propto d$, one finds by expanding the expressions in the brackets that $(\Delta f_p/f)_{sm} \propto d$ and $\Delta(1/2Q_p)_{sm} \propto d^3$. The signals decrease when thinner samples are measured. This behavior was shown in Fig. 8. Practically they become unobservable for thin films as pointed out above.

The situation is different in the electric case. It was pointed out in the preceding section that the expansions in Eqs. (60),(61) would yield a divergence of the signals in thin films. This would be unphysical and we have to reexamine the case. One has to recall that for the slab geometry in the electric case the depolarizing effect plays an important role. Therefore, $H_{\parallel e}$ is not independent of the film thickness. In Eq. (14) we need both the unperturbed and perturbed fields. For the unperturbed field one finds the boundary condition in Eq. (36). From Eq. (15) we found $D_p = D_0/N_e$ where the depolarizing factor depends on d . Thus, $H_{\parallel e}$ for the unperturbed field depends on d/N_e . For the perturbed fields in Eq. (14) one finds the boundary condition with D replacing D_p in Eq. (36). As we explained in Sec. II, when N_e is not extremely small one finds that $D \approx D_p$. It ensues that $H_{\parallel e}$ given by Eq. (36) can be taken also as the boundary condition of the perturbed field. This was the case treated in the preceding section. It brings about $H_{\parallel e}^2$ in the filling factor in Eqs. (60), (61). Now we may examine the case of extremely thin films ($d \rightarrow 0$) so that the depolarizing factor becomes very small

($N_e \rightarrow 0$). The unperturbed field D_p diverges while $H_{\parallel e}$ remains finite. This is obvious from the inspection of Eqs. (35), (36) where D_p is the slope of the variation of H_p . The perturbed field D saturates for $N_e \rightarrow 0$ (see Sec. II) so that the boundary magnetic field decreases linearly when $d \rightarrow 0$. As a result the signal amplitudes do not diverge but saturate at some high value.

One can make a numerical analysis if the thin film sample is approximated to an ellipsoid with principal axes L_x, L_y , and d . The electric field is along the y axis as in Fig. 3. The depolarizing factor is then given by an integral³²

$$N_e = N_{L_y} = \frac{L_x L_y d}{2} \int_0^\infty \frac{ds}{(s + L_y^2) \sqrt{(s + L_x^2)(s + L_y^2)(s + d^2)}}, \quad (62)$$

which can be evaluated numerically. The signal amplitude is

$$S_e(d) \propto \frac{d}{N_e} \left[\frac{\epsilon_r d}{1 + (\epsilon_r - 1) N_e} \right] d \cdot \mathcal{F}_e(d), \quad (63)$$

where only the dependence on d is pointed out. It includes in order the unperturbed field, the perturbed field, the volume of the sample, and the function $\mathcal{F}_e(d)$ which stands for the expression in the brackets of Eqs. (60),(61). We can choose some typical size parameters for thin films which are used in microwave measurements. Let $L_x = 1$ mm and $L_y = 3$ mm. The sample thickness is varied from 0.1 mm to the zero limit. The relative permittivity ϵ_r in Eq. (63) is not the permittivity of the nonperfect conducting sample treated here but stands for the nonperfect dielectric with the same boundary value problem (see Sec. II). We may replace it by $|\tilde{\sigma}|/\epsilon_0 \omega$ which gives the ratio of the induced current density in the conductor to the vacuum displacement current. A typical value is 10^7 at microwave frequencies. Experimentally one observes a step in the absorption curve when the sample is cooled from above T_c to zero temperature. At $T=0$ the absorption must vanish as can be seen from Eq. (61) in the limit $\lambda_2 \rightarrow 0$. Therefore, we need to analyze the signal level in the normal state. We may choose a typical value of $5 \mu\text{m}$ for the microwave penetration depth δ_n just above T_c . With these parameters the dependence of the signal level on the sample thickness can be evaluated from Eq. (63). The result is shown in Fig. 10. One can observe that starting from thick samples ($d > \delta_n$) the reduction of the sample thickness first brings about a minimum in the signal amplitude, while for thin samples one finds a tremendous increase of the signal amplitude. At extremely small values of d the signal amplitude saturates. The dashed line in Fig. 10(a) shows the erroneous divergence which would appear if the perturbed field were not correctly treated in the limit of $d \rightarrow 0$.

The shape of the frequency shift signal changes dramatically from thick to thin samples. The frequency shift in the normal state is reduced and a large negative peak appears below T_c . As a good measure of the overall signal amplitude one can monitor the frequency shift at zero temperature [Fig. 10(b)]. Its behavior as a function of d is found to be similar as for the absorption signal level.

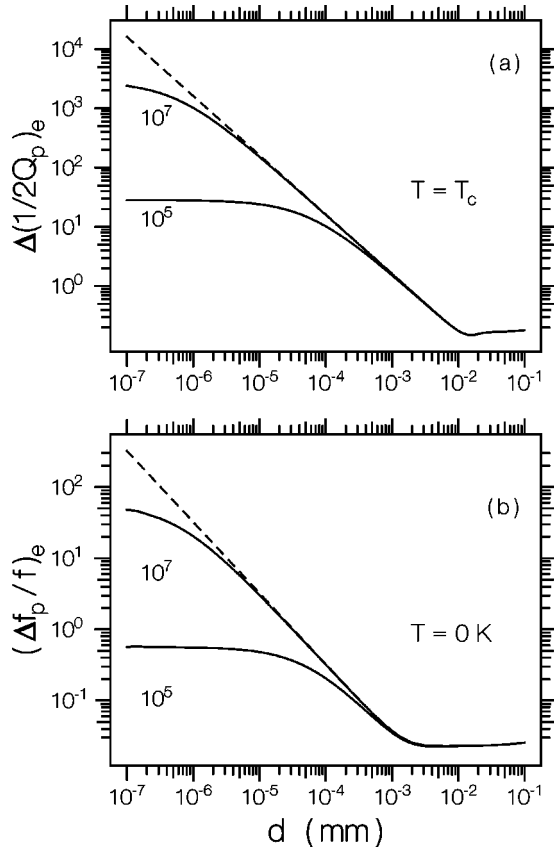


FIG. 10. The variation of (a) the absorption signal level at T_c and (b) frequency shift at zero temperature with the sample thickness d . The calculation was based on Eq. (63), and the parameters explained in the text. The curves are labeled by the values of $|\tilde{\sigma}|/\epsilon_0\omega$. If the perturbed field is not treated correctly, one obtains an erroneous divergence (dashed line).

VI. MICROWAVE EXPERIMENTS ON THIN FILMS

In order to provide experimental support to the theory in the preceding sections we have measured the absorption and frequency shift as a function of temperature in an $\text{YBa}_2\text{Cu}_3\text{O}_{7-\delta}$ epitaxial thin film on NdGaO_3 substrate. The thickness of the sample was 120 nm which is much less than the penetration depth $\delta_n(T_c) = 5 \mu\text{m}$. A cylindrical TE_{111} cavity was used. We have introduced an asymmetry in the cavity so that the degeneracy of the modes was lifted. Experiments were performed in two orthogonal modes with well separated resonance frequencies. The thin film sample could be mounted on a flat sapphire holder at various positions along the axis of the cavity. In the center of the cavity, the longer side (3 mm) of the film was along the electric field of mode I (higher frequency mode) and the shorter side (1 mm) was along the cavity axis. In this configuration the electric field of mode II (lower frequency mode) was perpendicular to the film plane. When the film was raised close to the top plate of the cavity the magnetic field of mode I was perpendicular to the film plane while the magnetic field of mode II was along the longer side of the film.

We used a BRUKER microwave bridge operating at 9–10 GHz. It has a built-in automatic frequency control (AFC) unit which tracks the klystron frequency always in resonance with the cavity. Thus, the frequency shift can be measured as

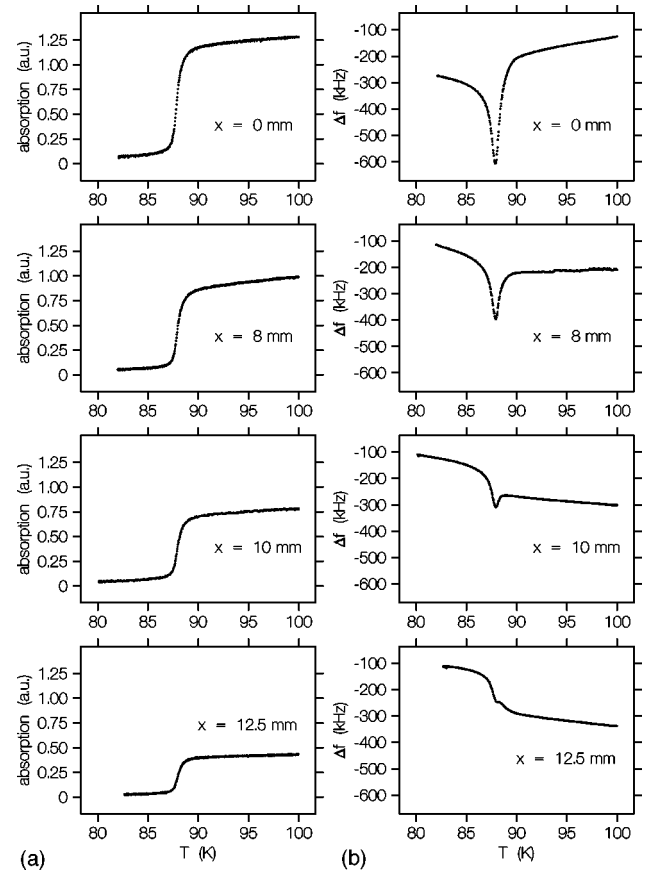


FIG. 11. Experimental signals of the temperature-dependent microwave absorption (a) and frequency shift (b) at various positions of the thin film in the cavity operating in mode I (see the text).

the temperature of the sample is varied. Simultaneously, changes in the absorption were measured by detecting the microwave diode current.

Figure 11 shows the temperature dependence of absorption and frequency shift measured at various positions of the sample along the cavity axis for mode I. The absorption signals change significantly only in amplitude but not in shape. However, the form of the frequency signals changes dramatically. Obviously the signals in the center of the cavity show the features due to the electric case as in Fig. 8. The signal is strong because the electric field is parallel to the longer side of the sample so that the depolarization effect is large. As the sample is placed at a higher position in the cavity the signal gradually loses electric and gains a magnetic component. Note that the magnetic field in mode I is perpendicular to the film plane so that the film acts as a thick sample (with some demagnetizing factor) and the shape of the magnetic signal is as shown in Fig. 7.

Measurements in mode II taken at the same positions of the sample in the cavity were also performed. The intention was to examine also the signals in the configuration which is opposite to the first, i.e., when the electric field is perpendicular to the film and the magnetic one is in the film plane. The measurements did not yield detectable signals. This is in agreement with the expectations based on the theory in the preceding sections. Namely, when the microwave electric field is perpendicular to the film the field \mathbf{D}_p in the sample is not much larger than the empty cavity field \mathbf{D}_0 . Therefore,

the induced magnetic field is so small that the signals turn out to be unobservable. Similarly, when the magnetic field is parallel to the film plane and the thickness of the film is much smaller than the penetration depth the shielding current is negligible and the signal is unobservably small.

It is also possible to orientate the sample in such a way that both the electric and magnetic fields are always in the film plane. This is achieved upon rotation of the film by 90° around the longer side (3 mm). The electric field in mode I coincides with this axis so that the electric contribution to the signal remains unchanged. On the contrary, the magnetic field in mode I lies in the film plane and yields no detectable signal. Consequently one observes only the electric signal which becomes weaker when the sample is raised from the center to the top plate of the cavity. When mode II is turned on for the same sample orientation the electric field is along the shorter side (1 mm) of the film. The observed signal has the same features as in mode I but the amplitude of the signal is stronger reduced due to the lower depolarization effect. The magnetic field in mode II is again in the film plane and yields no detectable signal. To summarize, when both fields are in the film plane one observes only the electric signal. Close to the magnetic field maximum the signal is reduced, but its shape still reveals the electric signal. We have also observed that thinner films yielded stronger signals.¹³

VII. RELATION TO AC SUSCEPTIBILITY

We have pointed out in this paper that microwave cavity perturbation measurement yields the average relative permeability $\tilde{\mu}_r = 1 + \tilde{\chi}_m$ of the sample when the driving field is the microwave magnetic field. Alternatively and much more frequently, ac susceptibility $\tilde{\chi}_m$ is measured at low frequencies ($10 - 10^5$ Hz) using the induction coil method. It may be of interest to clarify the relationship between the two techniques.

In the previous sections we have described the temperature dependences of $(\Delta f_p/f)_m$ and $\Delta(1/2Q_p)_m$ for a superconductor in the absence of a dc external magnetic field. In ac susceptibility measurements the sample is placed in a dc magnetic field \mathbf{H}_{dc} and a small ac field $\mathbf{H}_{ac}\exp(i\omega t)$ is superimposed. Microwave measurements can also be made with the sample exposed to a dc field \mathbf{H}_{dc} .^{21,36-39} The two techniques can, under these circumstances, be treated from an unique viewpoint, the only difference being the frequency scale.

We shall consider the cases when the applied dc field is much larger than the lower critical field, $\mathbf{B}_{dc} \gg \mathbf{B}_{c_1}$, so that the internal flux density in the mixed state is $\mathbf{B}_{dc} \approx \mu_0 \mathbf{H}_{dc}$. We also assume that it is practically constant throughout the sample as in a field cooled experiment. When the driving ac field is superimposed parallel to the dc field the induced current is perpendicular to the vortices, so that the Lorentz force exerts oscillations of the vortices around their equilibrium positions. In this case the induced current is carried by a combined motion of both superconducting and normal electrons, and the effective complex conductivity is given by^{19,20}

$$\frac{1}{\tilde{\sigma}_{\text{eff}}} = \frac{1 - b(v/v_f)}{(1-b)(\sigma_1 - i\sigma_2) + b\sigma_n} + \frac{b}{\sigma_n} \left(\frac{v}{v_f} \right), \quad (64)$$

where $b(T) = B_{dc}/B_{c_2}(T)$ is the reduced field, $\sigma_1(T) - i\sigma_2(T)$ is the complex conductivity of the Meissner state, and $\sigma_n(T)$ is the normal state conductivity in the vortex core. The ratio of the actual vortex velocity v to the maximum velocity v_f in the flux flow regime is the mobility factor which results from complicated flux dynamics processes.³⁹⁻⁴⁴ Since the study of the flux dynamics is not in the focus of the present paper we consider just the simple flux flow limit $v/v_f = 1$. Our aim is to show that the steplike absorption curves at microwave frequencies gradually change shape into the familiar ac-susceptibility curves with a peak below T_c only due to their different frequencies.

The phenomenology of current and field penetration described in the previous sections can be adapted to the present case straightforwardly. The effective complex conductivity $\tilde{\sigma}_{\text{eff}} = \sigma'_{\text{eff}} - i\sigma''_{\text{eff}}$ replaces $\tilde{\sigma} = \sigma_1 - i\sigma_2$ in the calculation of λ_1 and λ_2 in Eq. (55), and the complex permeability $\tilde{\mu}_r$ follows from Eqs. (56)–(58). However, the complexity of $\tilde{\sigma}_{\text{eff}}$ in Eq. (64) brings about new features which have to be discussed.

At the superconducting transition the reduced field is $b = 1$ so that the effective conductivity in Eq. (64) equals σ_n as expected. At lower temperatures b is reduced from unity towards the zero temperature value $b(0) = B_{dc}/B_{c_2}(0)$.

From Eq. (64) one can see that just below T_c , $\tilde{\sigma}_{\text{eff}}$ must become complex. However, σ_2 grows below T_c , and when the condition $\sigma_2 \gg \sigma_1$, σ_n/b is attained, the first term in Eq. (64) becomes approximately equal to i/σ_2 and is smaller than the second term. The effective conductivity is then practically real, even though the sample is in the superconducting state. Namely, the response of the superconductor in the mixed state to the ac field consists predominantly in the viscous vortex motion so that the conductivity is real. The above condition is frequency dependent since $(1/\sigma_2) = \mu_0 \omega \lambda_L^2$. For the same λ_L at a given temperature $T < T_c$, σ_2 can have orders of magnitude different values. At low frequencies, as commonly used in the measurements of ac susceptibility, σ_2 is very large and the first term in Eq. (64) is negligible with respect to the second. Hence, the effective conductivity is practically real above and below T_c . There is, however, a change in its temperature dependence. Above T_c the temperature dependence is that of $\sigma_n(T)$, while below T_c one has a real $\sigma_{\text{eff}} \approx \sigma_n B_{c_2}/B_{dc}$ which increases much faster than $\sigma_n(T)$ due to the temperature dependence of $B_{c_2}(T)$. Hence, the resulting penetration depth may rapidly decrease below the size of the sample and one observes a peak in the absorption curve as predicted from Eq. (34). This crossover from an electromagnetically thin to thick sample is field and frequency dependent because of the field and frequency dependency of σ_{eff} . At microwave frequencies this peak below T_c is not observed because σ_2 is orders of magnitude smaller, so that the first term in Eq. (64) does not become negligible immediately below T_c , i.e., $\tilde{\sigma}_{\text{eff}}$ remains complex. Figure 12 shows a set of curves for the same low temperature reduced field $b(0) = 10^{-4}$, but for several

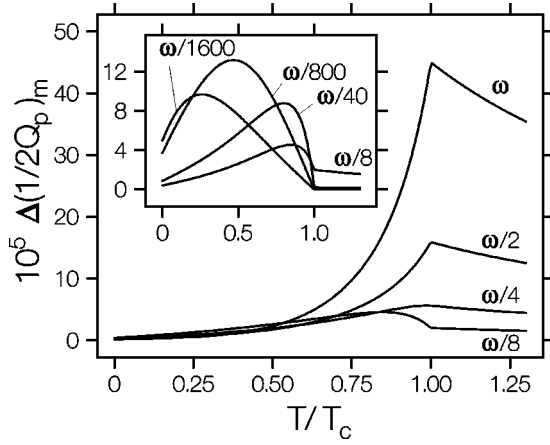


FIG. 12. The real and imaginary parts of the complex permeability $\tilde{\mu}_r$ calculated from Eqs. (57),(58) with σ_{eff} from Eq. (64). We take $b(0) = 10^{-4}$ and $d = 0.3\delta_n(T_c)$. The frequency ω is a typical microwave frequency. The labels indicate lower frequencies.

different frequencies. For the microwave frequency we choose $[\sigma_2(0)/\sigma_n(T_c)] = 25$ as in Sec. IV, and for lower frequencies we take the values which grow inversely with frequency. One can observe that when the frequency is lowered the steplike absorption curve at high frequencies gradually changes shape into a curve with a peak at lower frequencies. The detailed shape of the absorption curve observed in an ac susceptibility measurement reflects the actual flux dynamics in the sample.⁴⁰⁻⁴⁴

VIII. CONCLUSIONS

We have analyzed the cavity perturbation due to a conducting sample. It was shown that the conventional picture of the empty cavity as the unperturbed state was not satisfactory. An unperturbed state consisting of the cavity and a perfect conductor sample was introduced. Differences in the signal response between the positions of maximum magnetic and maximum electric field were clarified. Different treatments of the magnetic and dielectric properties of the sample were presented in order to avoid possible confusion when applying different perturbation equations. Also, the boundary conditions for the fields in the sample were analyzed and in particular their eventual changes with the conductivity of the sample. Explicit expressions are derived for the sample in the slab geometry for both magnetic and electric field positions. When the thickness d of the sample is much larger than the normal state penetration depth δ_n the losses and frequency shifts in both sample positions vary linearly with δ_n . Dramatic differences are found for thin films in which $d \ll \delta$. The losses due to the imposed magnetic microwave field are significantly reduced and follow the law $\Delta(1/2Q)_{nm} \sim \delta_n^{-2}$. On the contrary, at the electric field position one finds $\Delta(1/2Q)_{ne} \sim \delta_n^2$. The former becomes experimentally undetectable. This holds also in thin superconducting films. It is shown that the best choice for measuring the losses in thin film samples is the position of maximum electric field in the cavity. The frequency shift in that position shows a remarkable peak just below T_c . We have demonstrated these predictions by microwave measurements on an $\text{YBa}_2\text{Cu}_3\text{O}_{7-\delta}$ thin film at various positions in the cavity

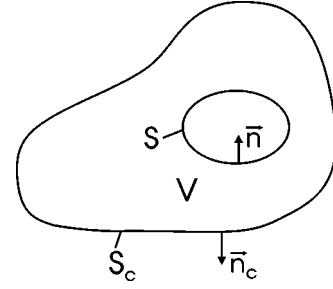


FIG. 13. Cavity with sample inside it. S_c and S are the surfaces of the cavity walls and sample, respectively. \mathbf{n}_c and \mathbf{n} are unit vectors which point out of the enclosed volume V .

from the electric field maximum to the magnetic field maximum. A relation of microwave measurements to ac susceptibility measurements was also discussed.

ACKNOWLEDGMENTS

D.-N.P. and B.N. acknowledge support by the Deutsche Forschungsgemeinschaft (DFG) Project No. Me362/14-1. We are thankful to H.-J. Kümmerer for helping us use the commercial MAFIA program. A.D., M.P., and D.P. acknowledge support from the Croatian Ministry of Science, Volkswagen Stiftung (Project No. I/71038), and DFG. The authors thank H.-U. Habermeier for providing the thin film sample for the measurements.

APPENDIX: PERTURBATION APPROACH

Let us assume a cavity with a perfect conductor placed inside and consider the fields of a mode formed in the volume V between the cavity walls and the sample (Fig. 13). The Maxwell equations in this case can be expressed as $\nabla \times \mathbf{E}_p = -i\tilde{\omega}_p \mathbf{B}_p$ and $\nabla \times \mathbf{H}_p = i\tilde{\omega}_p \mathbf{D}_p$ where the time dependence of the fields is $\exp(i\tilde{\omega}_p t)$. The complex frequency is $\tilde{\omega}_p = \omega_p(1 + i/2Q_p)$ where ω_p is the real frequency and Q_p is the Q factor determined by the losses in the cavity walls. One can use the operator algebra and Maxwell equations to prove that

$$\begin{aligned} & \int_V [\nabla \cdot (\mathbf{E}_p^* \times \mathbf{H}_p) + \nabla \cdot (\mathbf{E}_p \times \mathbf{H}_p^*)] d^3\mathbf{r} \\ &= -i(\tilde{\omega}_p - \tilde{\omega}_p^*) \int_V (\epsilon_0 \mathbf{E}_p \cdot \mathbf{E}_p^* + \mu_0 \mathbf{H}_p \cdot \mathbf{H}_p^*) d^3\mathbf{r}. \end{aligned} \quad (\text{A1})$$

The volume integral on the left hand side can be transformed into the integral over the surface enclosing the volume V

$$\begin{aligned} & \int_V [\nabla \cdot (\mathbf{E}_p^* \times \mathbf{H}_p) + \nabla \cdot (\mathbf{E}_p \times \mathbf{H}_p^*)] d^3\mathbf{r} \\ &= \oint_{S_c} [\mathbf{E}_p^* \times \mathbf{H}_p + \mathbf{E}_p \times \mathbf{H}_p^*] \cdot \mathbf{n}_c ds_c \\ &+ \oint_S [\mathbf{E}_p^* \times \mathbf{H}_p + \mathbf{E}_p \times \mathbf{H}_p^*] \end{aligned} \quad (\text{A2})$$

where S_c and S are the surfaces of the cavity walls and the sample, respectively. The second surface integral vanishes because \mathbf{E}_p is normal to the surface of a perfect conductor. Thus, Eq. (A1) can be written in the form

$$\oint_{S_c} [\mathbf{E}_p^* \times \mathbf{H}_p + \mathbf{E}_p \times \mathbf{H}_p^*] \cdot \mathbf{n}_c ds_c = \frac{\omega_p}{Q_p} W_{cp}, \quad (\text{A3})$$

where we have used W_{cp} to denote the energy of the fields in the cavity with the perfect conductor sample.

The perturbation consists in making the sample a nonperfect conductor. The Maxwell equations for the new fields are $\nabla \times \mathbf{E} = -i\tilde{\omega}\mathbf{B}$ and $\nabla \times \mathbf{H} = i\tilde{\omega}\mathbf{D}$ where $\tilde{\omega} = \omega(1 + i/2Q)$ is the shifted complex frequency. We can consider a volume integral containing products of unperturbed and perturbed fields and find

$$\begin{aligned} & \int_V [\nabla \cdot (\mathbf{E}_p^* \times \mathbf{H}) + \nabla \cdot (\mathbf{E} \times \mathbf{H}_p^*)] d^3\mathbf{r} \\ &= -i(\tilde{\omega} - \tilde{\omega}_p^*) \int_V (\epsilon_0 \mathbf{E} \cdot \mathbf{E}_p^* + \mu_0 \mathbf{H} \cdot \mathbf{H}_p^*) d^3\mathbf{r}. \end{aligned} \quad (\text{A4})$$

When the divergence theorem is used one obtains

$$\begin{aligned} & \int_V [\nabla \cdot (\mathbf{E}_p^* \times \mathbf{H}) + \nabla \cdot (\mathbf{E} \times \mathbf{H}_p^*)] d^3\mathbf{r} \\ &= \oint_{S_c} [\mathbf{E}_p^* \times \mathbf{H} + \mathbf{E} \times \mathbf{H}_p^*] \cdot \mathbf{n}_c ds_c \\ &+ \oint_S [\mathbf{E}_p^* \times \mathbf{H} + \mathbf{E} \times \mathbf{H}_p^*] \cdot \mathbf{n}_s ds. \end{aligned} \quad (\text{A5})$$

When the sample becomes a nonperfect but still a good conductor the fields are slightly changed at the sample surface and in its vicinity, but not at the cavity walls which are assumed to be relatively far away. Under these conditions one can replace the fields \mathbf{E} and \mathbf{H} in the integral over S_c in Eq. (A5) by \mathbf{E}_p and \mathbf{H}_p , respectively. This integral then becomes equal to Eq. (A3). In the integral over the sample surface S in Eq. (A5) only the second term remains. It is due to the fact that the perturbed field \mathbf{E} is not strictly perpendicular to the sample surface but has a small tangential component. Turning now the attention to the volume integral on the right-hand side of Eq. (A4) one can say that close to the sample the perturbed fields differ from the unperturbed ones by small perpendicular components, while the parallel components are only slightly changed. Farther from the sample even these differences vanish. Hence, one can replace \mathbf{E} and \mathbf{H} by \mathbf{E}_p and \mathbf{H}_p , respectively, and the integral becomes W_{cp} . With the above approximations one can write Eq. (A4) in the form

$$\frac{\omega_p}{Q_p} W_{cp} + \oint_S (\mathbf{E} \times \mathbf{H}_p^*) \cdot \mathbf{n}_s ds = -i(\tilde{\omega} - \tilde{\omega}_p^*) W_{cp}. \quad (\text{A6})$$

It leads to the final form for the complex frequency shift

$$\frac{\Delta \tilde{\omega}_p}{\omega} = \frac{(\tilde{\omega} - \tilde{\omega}_p)}{\omega} = \frac{i}{\omega W_{cp}} \oint_S (\mathbf{E} \times \mathbf{H}_p^*) \cdot \mathbf{n}_s ds. \quad (\text{A7})$$

*On leave of absence from: National Institute of Material Science, POB M.G.-7, RO-79600, Bucharest, Romania.

[†]Electronic address: d.peligrad@physik.uni-stuttgart.de

[‡]Present address: Rheinische Landes- und Hochschulklinik, Universität Düsseldorf, 40629 Düsseldorf.

[§]Electronic address: dulcic@faust.irb.hr

¹J. P. Carini, A. M. Awasthi, W. Beyermann, G. Grüner, T. Hylton, K. Char, M. R. Beasley, and A. Kapitulnik, *Phys. Rev. B* **37**, 9726 (1988).

²N. Klein, G. Müller, H. Piel, B. Roas, L. Schultz, U. Klein, and M. Peiniger, *Appl. Phys. Lett.* **54**, 757 (1989).

³L. Drabeck, G. Grüner, J.-J. Chang, A. Inam, X. D. Wu, L. Nazar, T. Venkatesan, and D. J. Scalapino, *Phys. Rev. B* **40**, 7350 (1989).

⁴N. Klein, H. Chaloupka, G. Müller, S. Orbach, H. Piel, B. Roas, L. Schultz, U. Klein, and M. Peiniger, *J. Appl. Phys.* **67**, 6940 (1990).

⁵L. Drabeck, K. Holczer, G. Grüner, J.-J. Chang, D. J. Scalapino, A. Inam, X. D. Wu, L. Nazar, and T. Venkatesan, *Phys. Rev. B* **42**, 10 020 (1990).

⁶D. W. Cooke, E. R. Gray, H. H. S. Javadi, R. J. Houlton, B. Rusnak, E. A. Meyer, P. N. Arendt, N. Klein, G. Müller, S. Orbach, H. Piel, L. Drabeck, G. Grüner, J. Y. Josefowicz, D. B. Rensch, and F. Krajenbrink, *Solid State Commun.* **73**, 297 (1990).

⁷E. Silva, M. Lanucara, and R. Marcon, *Supercond. Sci. Technol.* **9**, 934 (1996).

⁸J. R. Waldram, M. Robson, H.-M. Cheah, and R. E. Somekh, *Supercond. Sci. Technol.* **4**, S214 (1991).

⁹D. E. Oates and A. C. Anderson, *IEEE Trans. Magn.* **27**, 867 (1991).

¹⁰L. D. Chang, M. J. Moskowitz, R. B. Hammond, M. M. Eddy, W. L. Olson, D. D. Casavant, E. J. Smith, M. Robinson, L. Drabeck, and G. Grüner, *Appl. Phys. Lett.* **55**, 1357 (1989).

¹¹R. B. Hammond, G. V. Negrete, L. C. Bourne, D. D. Strother, A. H. Cardona, and M. M. Eddy, *Appl. Phys. Lett.* **57**, 825 (1990).

¹²A. Inam, X. D. Wu, L. Nazar, M. S. Hegde, C. T. Rogers, T. Venkatesan, R. W. Simon, K. Daly, H. Padamsee, J. Kirchgessner, D. Moffat, D. Rubin, Q. S. Shu, D. Kalokitis, A. Fathy, V. Pendrick, R. Brown, B. Brycki, E. Belohoubek, L. Drabeck, G. Grüner, R. Hammond, F. Gamble, B. M. Lairson, and J. C. Bravman, *Appl. Phys. Lett.* **56**, 1178 (1990).

¹³G. Schaumburg, H. W. Helberg, P. Berberich, and H. Kinder, *Ann. Phys. (Leipzig)* **1**, 584 (1992).

¹⁴G. Schaumburg and H. W. Helberg, *J. Phys. III* **4**, 917 (1994).

¹⁵N. Klein, U. Dähme, U. Poppe, N. Tellmann, K. Urban, S. Orbach, S. Hensen, G. Müller, and H. Piel, *J. Supercond.* **5**, 195 (1992).

¹⁶N. Klein, N. Tellmann, H. Schulz, K. Urban, S. A. Wolf, and V. Z. Kresin, *Phys. Rev. Lett.* **71**, 3355 (1993).

¹⁷Z. Ma, R. C. Taber, L. W. Lombardo, A. Kapitulnik, M. R. Beasley, P. Merchant, C. B. Eom, S. Y. Hou, and J. M. Phillips, *Phys. Rev. Lett.* **71**, 781 (1993).

- ¹⁸H. E. Porteanu, K. Karrai, R. Seifert, F. Koch, P. Berberich, and H. Kinder, Phys. Rev. Lett. **75**, 3934 (1995).
- ¹⁹A. Dulčić and M. Požek, Fizika (Zagreb) **A2**, 43 (1993).
- ²⁰A. Dulčić and M. Požek, Physica C **218**, 449 (1993).
- ²¹I. Ukrainczyk and A. Dulčić, Europhys. Lett. **28**, 199 (1994).
- ²²C. Kessler, B. Nebendahl, D.-N. Peligrad, A. Dulčić, H.-U. Haberman, and M. Mehring, Physica C **219**, 233 (1994).
- ²³H. A. Bethe and J. Schwinger, N.D.R.C. Report No. D1-117, Cornell University, 1943 (unpublished).
- ²⁴E. G. Spencer, R. C. LeCraw, and L. A. Ault, J. Appl. Phys. **28**, 130 (1957).
- ²⁵R. A. Waldron, *Theory of Guided Electromagnetic Waves* (Reinhold, London, 1969).
- ²⁶K. Simonyi, *Theoretische Elektrotechnik*, 9th ed. (VEB Deutscher Verlag der Wissenschaften, Berlin, 1989).
- ²⁷S.-H. Chao, IEEE Trans. Microwave Theory Tech. **MTT-33**, 519 (1985).
- ²⁸MAFIA version 3.20, 1994, Solution of Maxwell's equations by Finite Integration Algorithms, a commercial, interactive program package for the computation of electromagnetic fields which uses the finite integration technique (unpublished).
- ²⁹E. H. Brandt, Phys. Rev. Lett. **74**, 3025 (1995).
- ³⁰J. A. Osborn, Phys. Rev. **67**, 351 (1945).
- ³¹M. Cohen, S. K. Khanna, W. J. Gunning, A. F. Garito, and A. J. Heeger, Solid State Commun. **17**, 367 (1975).
- ³²C. J. F. Böttcher, *Theory of Electric Polarization*, 2nd ed. (Elsevier, Amsterdam, 1973), Vol. 1.
- ³³A. M. Portis, *Electromagnetic Fields: Sources and Media* (Wiley, New York, 1978).
- ³⁴J. D. Jackson, *Classical Electrodynamics*, 2nd ed. (Wiley, New York, 1987).
- ³⁵M. W. Coffey and J. R. Clem, Phys. Rev. B **45**, 9872 (1992).
- ³⁶J. I. Gittleman and B. Rosenblum, Proc. IEEE **52**, 1138 (1964).
- ³⁷J. I. Gittleman and B. Rosenblum, Phys. Rev. Lett. **16**, 734 (1966).
- ³⁸J. Owliaei, S. Sridhar, and J. Talvacchio, Phys. Rev. Lett. **69**, 3366 (1992).
- ³⁹M. Golosowsky, M. Tsindlekht, and D. Davidov, Supercond. Sci. Technol. **9**, 1 (1996).
- ⁴⁰E. H. Brandt, Phys. Rev. Lett. **67**, 2219 (1991); Physica C **195**, 1 (1992).
- ⁴¹M. W. Coffey and J. R. Clem, Phys. Rev. Lett. **67**, 386 (1991).
- ⁴²E. H. Brandt, Rep. Prog. Phys. **58**, 1465 (1995).
- ⁴³J. Kotzler, G. Nakielski, M. Baumann, R. Behr, F. Goerke, and E. H. Brandt, Phys. Rev. B **50**, 3384 (1994).
- ⁴⁴G. Blatter, M. V. Feigel'man, V. B. Geshkenbein, A. I. Larkin, and V. M. Vinokur, Rev. Mod. Phys. **66**, 1125 (1994).